Synthetic and Systems Biotechnology 8 (2023) 654–672

Contents lists available at ScienceDirect

Synthetic and Systems Biotechnology

journal homepage: www.keaipublishing.com/en/journals/synthetic-and-systems-biotechnology

Design and mathematical analysis of activating transcriptional amplifiers that enable modular temporal control in synthetic juxtacrine circuits

Calvin Lam [1,2]

ARTICLE INFO

Keywords:
Synthetic biology
Synthetic development
Synthetic immunotherapy
synNotch
SNIPR
Amplifiers
Self-organization
Temporal control
Spatiotemporal control
CAR T cell
Synthetic receptors

ABSTRACT

The ability to control mammalian cells such that they self-organize or enact therapeutic effects as desired has incredible implications. Not only would it further our understanding of native processes such as development and the immune response, but it would also have powerful applications in medical fields such as regenerative medicine and immunotherapy. This control is typically obtained by synthetic circuits that use synthetic receptors, but control remains incomplete. The synthetic juxtacrine receptors (SJRs) are widely used as they are fully modular and enable spatial control, but they have limited gene expression amplification and temporal control. As these are integral facets to cell control, I therefore designed transcription factor based amplifiers that amplify gene expression and enable unidirectional temporal control by prolonging duration of target gene expression. Using a validated *in silico* framework for SJR signaling, I combined these amplifiers with SJRs and show that these SJR amplifier circuits can direct spatiotemporal patterning and improve the quality of self-organization. I then show that these circuits can improve chimeric antigen receptor (CAR) T cell tumor killing against various heterogenous antigen expression tumors. These amplifiers are flexible tools that improve control over SJR based circuits with both basic and therapeutic applications.

1. Introduction

Synthetic biology is a rapidly expanding field with various subfields, with two notable subfields being synthetic development and synthetic immunotherapy [1–6]. In synthetic development, researchers are engineering mammalian cells to control self-organization; the goal is to further understanding of native developmental processes and regenerative therapeutics [1,4,5,7,8]. In a referential study, naïve fibroblasts were programmed with synthetic circuits such that individual cells could sense neighbors and self-organize into diversely patterned spheroids [9]. In synthetic immunotherapy, researchers focus on engineering immune cells to control therapeutic effects; the goal is to direct specific and novel immune responses [2,3,10–14]. Recent achievements include programming T cells with synthetic circuits that enable multi-antigen discrimination, localized activation, and/or select cytokine secretion [15–18].

Both subfields commonly rely on synthetic receptors to create the behavior-controlling synthetic circuits, with synthetic juxtacrine receptors (SJRs) such as synNotch and SNIPRs being widely used due to their remarkable modularity, high spatial control, and potential for clinical translation [9,15–22]. The SJR class of receptors have an extracellular domain that can be programmed to sense a ligand of choice and the intracellular domain programmed to control a gene of choice (Fig. 1A). When the SJR binds the juxtacrine target ligand on a neighboring surface, it releases an intracellular transcription factor to regulate the target gene [16,17,19] (Fig. 1B). Because of this stoichiometric mechanism, one transcription factor released per activated SJR, there is minimal amplification of target gene expression [19]. Furthermore, as the SJR is dependent on juxtacrine ligand on neighbors to maintain gene expression, target gene expression is highly localized. This allows excellent spatial control over cell behavior, but minimal control on the temporal axis (Fig. 1B) [16,19]. Thus, direct gene activation by SJRs neither enables amplification nor temporal regulation of target gene expression.

However, both expression amplification and temporal regulation are basic yet integral facets of numerous biological processes [23–28]. For example, expression amplification of Nanog and Oct4 via a feedback loop is critical for embryonic stem cell maintenance [27]. In the immune response to tumors, localized reservoirs of IL-2 serve to temporally enhance T cell activity [28]. Somite development in vertebrates is an

Peer review under responsibility of KeAi Communications Co., Ltd.
E-mail address: calvin.lam.k@gmail.com.
[1] Independent Investigator.
[2] Present Address: Department of Biochemistry and Molecular Biology, University of Nebraska Medical Center, Omaha, NE, 68198, USA.

https://doi.org/10.1016/j.synbio.2023.09.008
Received 3 June 2023; Received in revised form 9 August 2023; Accepted 25 September 2023
Available online 10 October 2023

intricate dance involving both amplification and temporal regulation [23–26]. As the goal of the subfields is to control such processes, it would be ideal if SJRs allowed for amplification and temporal regulation. Although the SJR's current use form, the direct activation circuit, neither enables amplification nor temporal regulation, it may still be possible through an intermediate component [16]. Across diverse native biological circuits, transcription factors are used to regulate one another and the target gene in an amplifier manner to achieve temporal regulation [27,29–31]. In synthetic circuits, transcription factors have been used to generate amplifier loops, allowing cells to retain memory of a stimulus [32]. As SJRs mechanistically function via transcription factors, I reasoned that a transcription factor based amplifier could amplify target gene expression and concurrently enable temporal regulation in SJR based circuits.

I therefore designed two generalizable transcription factor based amplifiers that enable expression amplification and temporal regulation. These amplifiers are driven by a SJR before they subsequently regulate target gene expression (Fig. 1C). In this amplifier subfamily, which amplifies gene expression and increases duration of gene expression, I designed two circuits. Both amplify gene expression but one temporarily prolongs gene expression (Temporarily Amplified Activation, Fig. 1E) while the other enables permanent gene expression (Permanently Amplified Activation, Fig. 1F). The SJR inhibition family and its amplifier variants, designed to amplify inhibition of gene expression and decrease duration of gene expression, is described in the upcoming accompanying paper.

In a previous work, my colleagues and I developed the GJSM (Generalized Juxtacrine Signaling Model), a set of mathematical

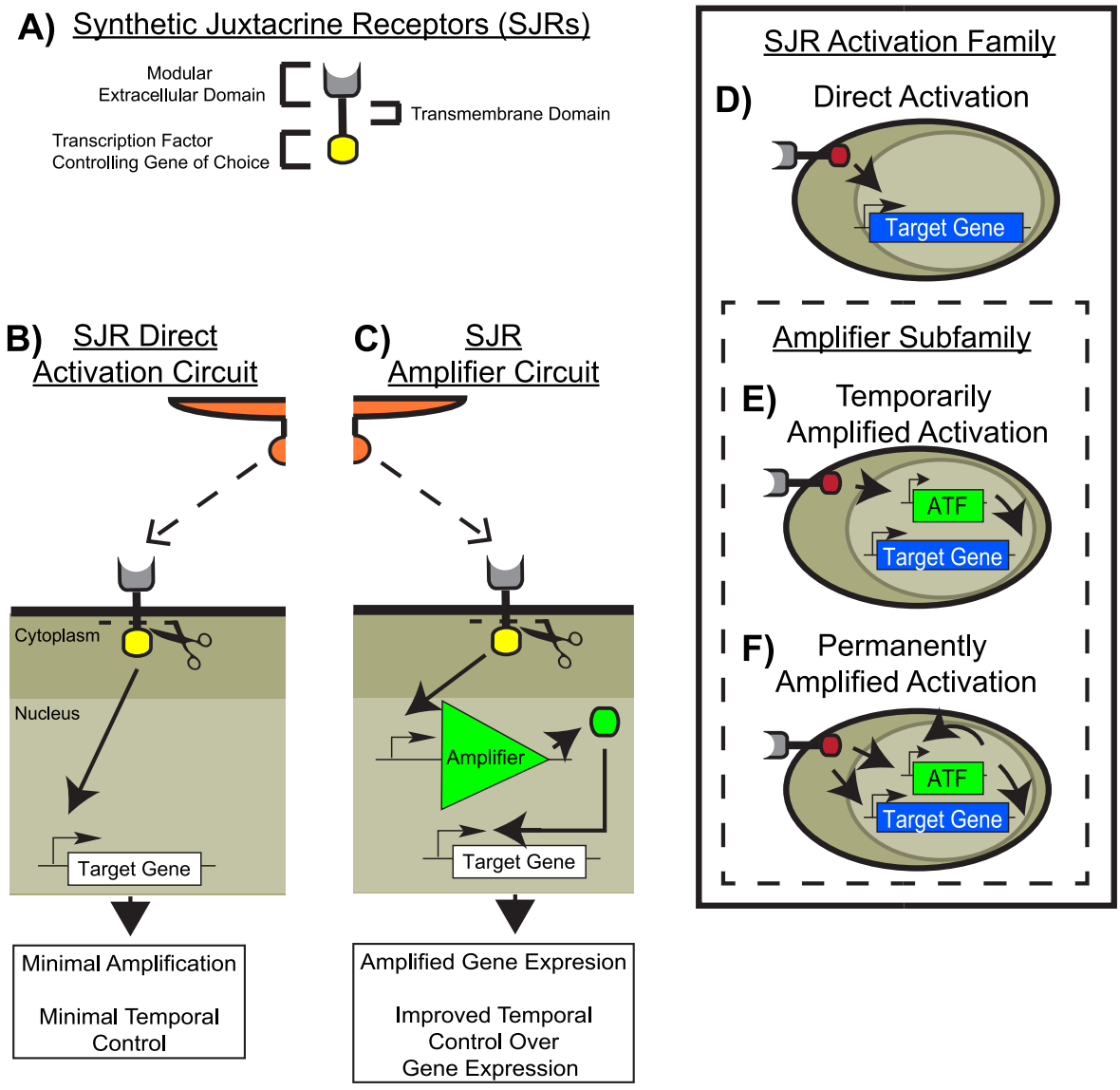

Fig. 1. Designing Amplifiers to Combine with SJRs for the SJR Amplifier Circuits. A) Synthetic juxtacrine receptors (SJRs) are a class of synthetic receptors modular in both extracellular domain and intracellular domain. The extracellular domain consists of a choice ligand binding domain, and the intracellular domain consists of a transcription factor controlling a gene of choice [9,15–21,36,37]. B) In the classic SJR direct activation circuit, the SJR binds its juxtacrine cognate ligand to release the transcription factor controlling the target gene. This stoichiometric mechanism results in minimal expression amplification and temporal regulation [16,19]. C) This could be overcome by having the SJR drive the expression of a transcription factor based amplifier that amplifies target gene expression and prolongs duration of expression. D) The SJR Activation Family of circuits investigated in this study, consisting of the stereotypical direct activation circuit and the amplifier imbued Amplifier Subfamily. E) The temporarily amplified activation circuit is designed to temporarily amplify and prolong duration of target gene expression. SJR drives expression of an activating transcription factor (ATF) that then drives expression of the target gene. F) In the permanently amplified activation circuit, the SJR drives expression of an ATF that can then drive itself and the target gene, which should enable amplification and permanent gene expression.

equations formulated to allow intuitive and simple modeling of SJR circuits. We showed that this model can faithfully model SJR circuits and when parameterized to an initial training set, can successfully predict the self-organized structures that arise from SJR circuits that drive differential adhesion [33]. This model development and validation study yielded a framework for computational exploration of SJR circuits, serving as a powerful tool for me to thoroughly explore and push the amplifier circuits designed in this study to their operational limits. The GJSM framework would enable rapid yet extensive investigation into circuit behavior across a variety of conditions. Using the framework, I converted the circuits into mathematical equations, then implemented the equations into *in silico* cells created in the cellular Potts model [26,34,35]. This is the *in silico* analog of transducing live cells with the analogous circuit genes (SFig.1A).

Here I show that the amplifiers are capable of amplifying target gene expression and increasing duration of gene expression. When combined with SJRs, these SJR amplifier circuits enable directing novel spatio-temporal patterning and improving self-organization in synthetic development. In synthetic immunotherapy, these circuits improve tumor cell killing. Though I focus here on two subfields, these amplifiers serve as versatile tools to temporally control and amplify gene expression for a broad range of synthetic biology applications.

2. Results

2.1. Design of the SJR amplifier circuits

Of the circuits in the SJR Activation Family, the direct activation circuit is the most well-known. It uses a synthetic juxtacrine receptor (SJR) that, upon binding its cognate ligand, releases a transcription factor that directly drives target gene expression (Fig. 1D) [9,15–21,36,37]. This design offers high spatial control, but with strong reliance on SJR signaling to maintain target gene expression, it offers little temporal control. Furthermore, due to SJR stoichiometry (one transcription factor (TF) per SJR), it offers little target gene expression amplification [16,19].

The Amplifier Subfamily is designed to add gene expression amplification along with temporal control to SJR based circuits (Fig. 1E and F). In the temporarily amplified activation circuit, the SJR drives expression of an activating transcription factor (ATF) that subsequently drives expression of the target gene (Fig. 1E). Gene expression amplification should be observed with higher gene product levels. Furthermore, continued increasing target gene expression should be observed even when SJR signaling is lost, provided that the ATF level remains sufficiently elevated to continue driving target gene expression. Thus, this temporarily amplified activation circuit should amplify and temporarily prolong target gene expression.

Amplification can also result in permanent gene expression. In the permanently amplified activation circuit, the transcription factor released by the SJR is identical to the ATF. Furthermore, both the ATF gene and target gene are activated by this ATF (controlled by same type of promoter) (Fig. 1F). Thus, with initial sufficient SJR signaling, ATF is expressed and drives ATF expression. As the target gene's promoter is also responsive to ATF, target gene expression should be amplified and permanently driven.

2.2. Amplifiers amplify and enable temporal control over target gene expression

With the SJR amplifier circuits designed, I converted the circuits to equations using the GJSM model [35] and implemented them into *in silico* cells defined via the Cellular Potts framework [26,34] (See Methods section for more details). I then tested their ability to amplify target gene expression and enable temporal control with a simple cell-cell signaling setup modified from Ref. [38]. Gray cells were programmed with either the direct activation circuit (Fig. 1D) or one of the amplifier circuits (Fig. 1E and F), with the SJR set to be responsive to orange ligand on orange cells and the target gene set to be a red reporter (Fig. 2A).

A single cubic gray cell was then seeded with 3 orange cubic cells such that one face of an orange cell contacted 1 gray cell face (Fig. 2B). Cells were frozen (static in volume, surface area, and morphology) to maintain uniform and constant SJR signaling. This cell-cell signaling setup enables controlling the exact orange ligand-SJR signal the gray cell receives and should therefore enable determining the amplificatory effects of the amplifiers. At 25000 timesteps, orange neighbors were deleted to test how SJR signaling loss would affect reporter expression (Fig. 2B). Both reporter and ATF levels (if applicable), were tracked throughout the course of the experiment.

In the GJSM model, different properties of gene expression are modelled by different parameters. With a circuit that activates gene expression, the parameter β models difficulty of gene expression, with higher values modeling higher expression difficulty. Lower β values allow easier gene expression but at the risk of leaky gene expression [35]. See Brief overview of Generalized Juxtacrine Signaling Model (GJSM) in the Methods Section or the original study [35] for more details.

With the reporter expression difficulty (β Reporter) set to 1000, the easiest tested expression difficulty without leakiness (SFig.2A), all circuits were able to yield reporter expression with 3 orange neighbors. Consistent with previous *in vitro* studies, the direct activation circuit had immediate reporter level decrease upon removal of the neighbors (Fig. 2C) [16,19]. In contrast, all of the amplifier circuits were able to maintain increasing reporter levels for some time after loss of SJR signaling (Fig. 2C). Moreover, these amplifier circuits were able to maintain higher reporter levels as well.

Challenging these circuits with higher reporter expression difficulties yielded similar results. Amplifier circuits did not have immediate reporter decrease upon loss of SJR signaling and at the same reporter expression difficulty level, provided that the reporter was expressed, consistently had higher reporter levels compared to the direct activation circuit (Fig. 2D). Similar results were obtained with 1 and 6 orange neighbors (data not shown). Of note, the temporarily amplified activation circuit failed at expression difficulties β Reporter$\geq$18000 while the permanently amplified activation circuit failed at $\geq$25000. This is expected as the ATF saturation level (parameter κ in GJSM) was set to 25000 in these simulations, making it extremely difficult to achieve amplification/expression as expression difficulties increases towards 25000. The operational limits of these circuits demonstrate that amplifier behavior is not guaranteed solely by circuit design but is dependent on parameters such as saturation/decay and expression difficulty. Nonetheless, with the same identical SJR signal that the direct activation circuit had, the amplifier circuits were able to amplify reporter expression to maintain higher reporter levels and prolong reporter expression.

Furthermore, these results confirm that the amplifier circuits operate temporally as designed. The temporarily amplified activation circuit only temporarily prolonged reporter expression, as reporter levels eventually decreased at all the reporter expression difficulties tested (Fig. 2C and D). This is due to the ATF's dependency on SJR signaling to remain elevated and sustain reporter expression (SFig.2B). There is also an expected temporal delay before reporter expression began as the ATF requires time to be expressed and sufficiently accumulate before being able to drive reporter expression. This delay increased as expression difficulty increased because the ATF requires more time to accumulate to higher levels.

The permanently amplified activation circuit demonstrated no notable decrease in reporter levels, confirming its capability to permanently drive target gene expression (Fig. 2C and D). This is due to the ATF being able to maintain elevated ATF levels via positive self-feedback (SFig.2B). There is also a temporal delay with this circuit before reporter expression began, again reflecting the need for ATF to be expressed and sufficiently accumulate before being able to drive reporter expression. As expected, this delay increased with increasing

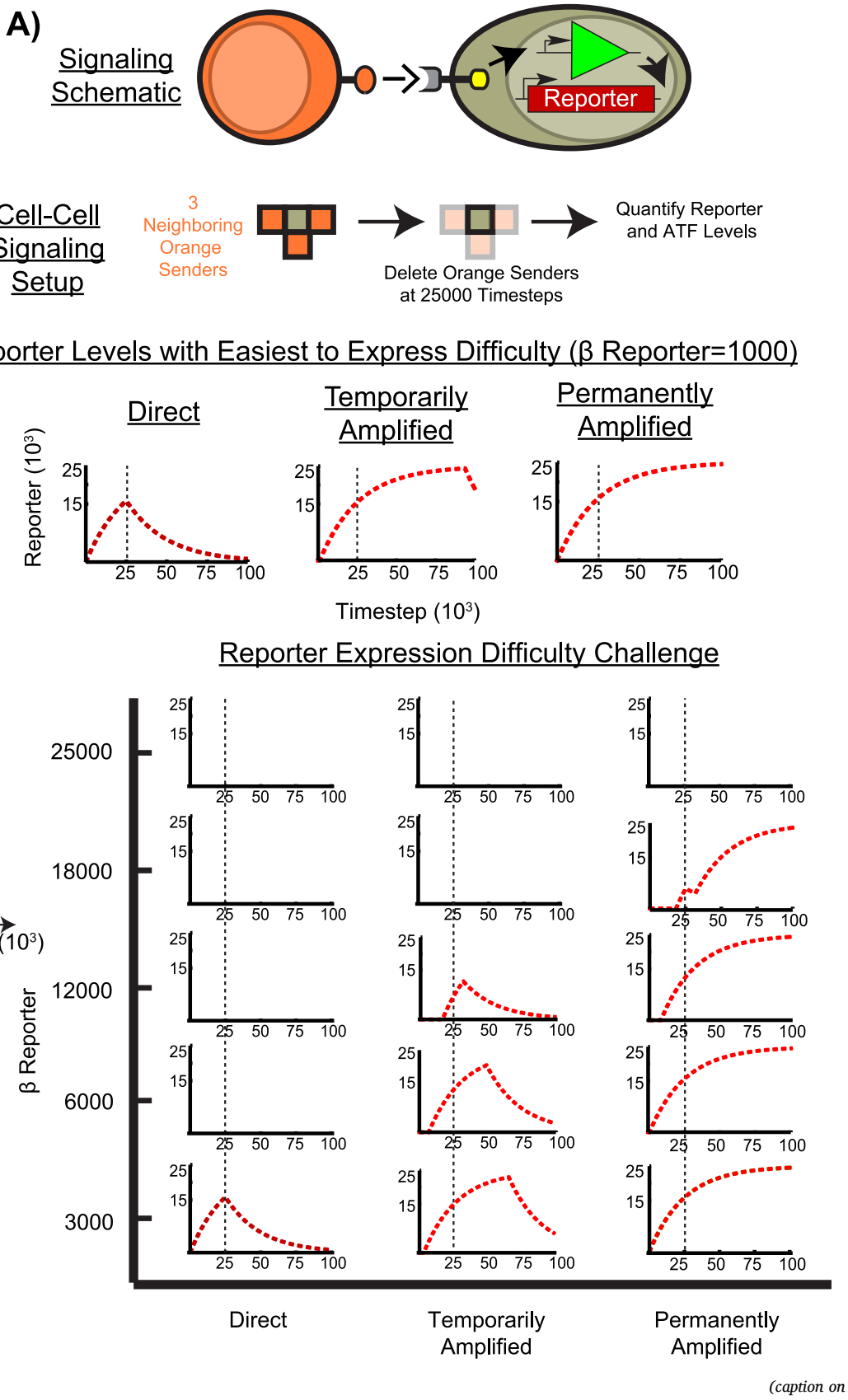

(caption on next page)

Fig. 2. Amplifiers Amplify and Enable Temporal Regulation Over Target Gene Expression. A) Signaling schematic used to test the amplifiers for their ability to amplify gene expression and enable temporal control of a red reporter. Gray cells receive signal from orange ligand on orange cells via an anti-(orange ligand) SJR that either drives red reporter expression directly (Direct Activation) or an amplifier (Temporarily Amplified or Permanently Amplified) that then drives red reporter expression. B) One cubic gray cell is seeded with 3 cubic orange cells and at 25000 timesteps, orange cells are deleted to determine effect on red reporter levels. Both reporter and ATF levels were tracked. Amplifiers should amplify reporter levels such that there should be continued increasing reporter levels immediately after SJR signal loss and higher reporter levels. C) Reporter traces from the different circuits. At the easiest reporter expression difficulty (β Reporter = 1000), directly activated cells had reporter expression decrease immediately after loss of orange cells while the amplifier imbued cells continued to increase reporter levels and maintain higher reporter levels. D) Reporter expression difficulty challenge. Reporter levels from challenging the cells with higher reporter expression difficulty, β Reporter, from 3000 to 25000. At the same expression difficulty, amplifier imbued cells had increasing reporter levels even after orange neighbors were lost and higher reporter levels, indicating amplification of target gene expression. These results also confirm the temporal design of circuits. The temporarily amplified activation circuit only temporarily prolongs reporter expression (decreases sometime later) while the permanently amplified circuit continues to prolong reporter expression. One trace shown per circuit/condition and simulations ran for 100,000 timesteps.

expression difficulty. However, the delay is less compared to the temporarily amplified activation circuit due to ATF positive self-feedback.

2.3. Spatial control from SJRs and temporal control from amplifiers enable spatiotemporal patterning

With evidence that the amplifiers are able to amplify target gene expression and enable temporal control, I next tested these circuits in synthetic development experiments as the direct activation circuit has been used extensively to drive self-organization [9]. In the reference study, naïve L929 mouse fibroblast cells were engineered with a variety of different direct activation circuits driving the expression of different cadherins, ligands, and reporters. As cells signaled to one another and sorted, they formed a variety of patterned structures. Of these structures, the multipole structure is of particular interest as it is an example of symmetry breaking in engineered development and by itself can give rise to different multipole structures (Fig. 3B). I therefore tested if the amplifier circuits could be used to generate a variety of spatiotemporal patterned multipole structures.

To achieve the multipole structures, I used the developmental trajectory in the original study [9]. From a mixture of orange and gray cells, gray cells receive signal from orange cells and become N-cadherin (Ncad) positive (blue cells) (Fig. 3A). These N-cadherin cells sort to one another as N-cadherin is a homotypic adhesive cadherin. These N-cadherin cells also signal back to orange cells, turning orange cells P-cadherin (Pcad) positive (red colored). P-cadherin cells are also homotypic adhesive and sort to one another. A mixture of these gray and orange cells results in a multipole structure with cores/poles of either N-cadherin$^+$ (Ncad$^+$) or P-cadherin$^+$ (Pcad$^+$) cells (Fig. 3B).

I began by testing how gray cells with either the direct or an amplifier circuit would affect spatiotemporal multipole patterning. I programmed gray cells with a SJR that responds to orange ligand on orange cells and drives either N-cadherin/blue ligand (gene is *NCAD/BLUE-L*) directly (direct activation circuit) or an amplifier that subsequently drives N-cadherin/blue ligand (amplifier circuits). This turns gray cells blue or cyan, representing the N-cadherin$^+$ blue ligand$^+$ state. Blue/cyan cells can now signal via blue ligand to orange cells, as they constitutively have anti-(blue ligand) SJR on their surface. This directly drives P-cadherin (gene is *PCAD*) expression in orange cells. The color key to the cells' states is given in Fig. 3C. Ncad is N-cadherin, Pcad is P-cadherin and ATF is activating transcription factor. These described circuit combinations are given in Fig. 3D. All circuits were programmed into *in silico* L929 (ISL929), an *in silico* cell line modelling the same murine L929s used in the original study and validated for modeling such structures [9,35]. GJSM parameters were set equal across all circuits.

Combining the orange cells with differently activated gray cells resulted in a variety of spatiotemporal patterned structures. Directly activated gray cells consistently formed a spatially sensitive pattern; blue cells were localized where they could contact cognate signaling orange/red cells while cells that lost contact deactivated to gray, forming the rest of the core/pole (Fig. 3D). A mixture of ~30 gray and ~30 orange cells yielded a blue stripe with a gray pole while ~90 gray and ~90 orange cells yielded a gray core with blue stripes proximal to orange/red cells (Fig. 3D).

Adding temporal control with temporarily amplified activated gray cells generated a spatiotemporal pattern; cyan cells were localized next to orange/red cells but amplifying and prolonging high N-cadherin/blue ligand expression allowed cells to remain blue (N-cadherin$^+$ blue ligand$^+$) even when they lost contact with orange/red cells (Fig. 3D). ~30 gray and ~30 orange cells generated cyan stripes with a blue pole while ~90 gray and ~90 orange cells formed a blue core with cyan stripes next to orange/red cells (Fig. 3D).

Adding temporal control with the permanently amplified activation circuit yielded a different spatiotemporal pattern; nearly all gray cells became cyan and cyan cells localized independent of contact with orange/red cells (Fig. 3D). These results are consistent with the permanently amplified activation circuit's design; it amplifies and drives permanent expression of the target gene, *NCAD/BLUE-L*, thus loss of contact with orange/red cells should not affect target gene expression. ~30 gray and ~30 orange cells generated cyan poles while ~90 gray and ~90 orange cells reliably formed cyan cores (Fig. 3D). Additional representative structures for all of the circuits are given in SFig.3.

These results demonstrate that different amplifiers confer different levels of temporal control and when combined with the spatial control conferred by SJRs, yield spatiotemporal circuits that can direct multicellular patterning.

2.4. Spatiotemporal patterning can be expanded with intercellular amplifier circuit combinations

In the multipole structures formed (Fig. 3D), orange cells consistently formed orange poles with a red stripe as they were programmed with only the direct activation circuit. I wondered what different spatiotemporal patterns could be achieved if orange cells were also imbued with an amplifier. To test this, I used the same setup and parameters for multipole structure formation (Fig. 3), but also expanded orange cells to have either the temporarily amplified activation circuit or the permanently amplified activation circuit. This allowed me to test the remaining combinations of circuits not tested in Fig. 3: gray (direct, temporarily amplified, permanently amplified) to orange (temporarily amplified, permanently amplified) (Fig. 4A). The color key to the cells' states is given in Fig. 4B. Pcad is P-cadherin, Ncad is N-cadherin and ATF is activating transcription factor.

Different circuit combinations with differently amplified cells broadly expanded the spatiotemporal patterns obtained in Fig. 3. Temporarily amplified activated orange cells allowed forming a pink, then red, and then orange stripe spatiotemporal pattern. When combined with directly activated gray cells, they allowed forming a 5-layered multipole structure (Fig. 4C). An additional layer could be obtained by combining them instead with temporarily amplified activated gray cells, allowing the formation of a 6-layered multipole structure (Fig. 4C). A 4-layered multipole structure could be obtained by combining them with permanently amplified activated gray cells (Fig. 4C). Using more cells (~90 gray and ~90 orange cells) yielded similar patterning but with additional poles (Fig. 4C).

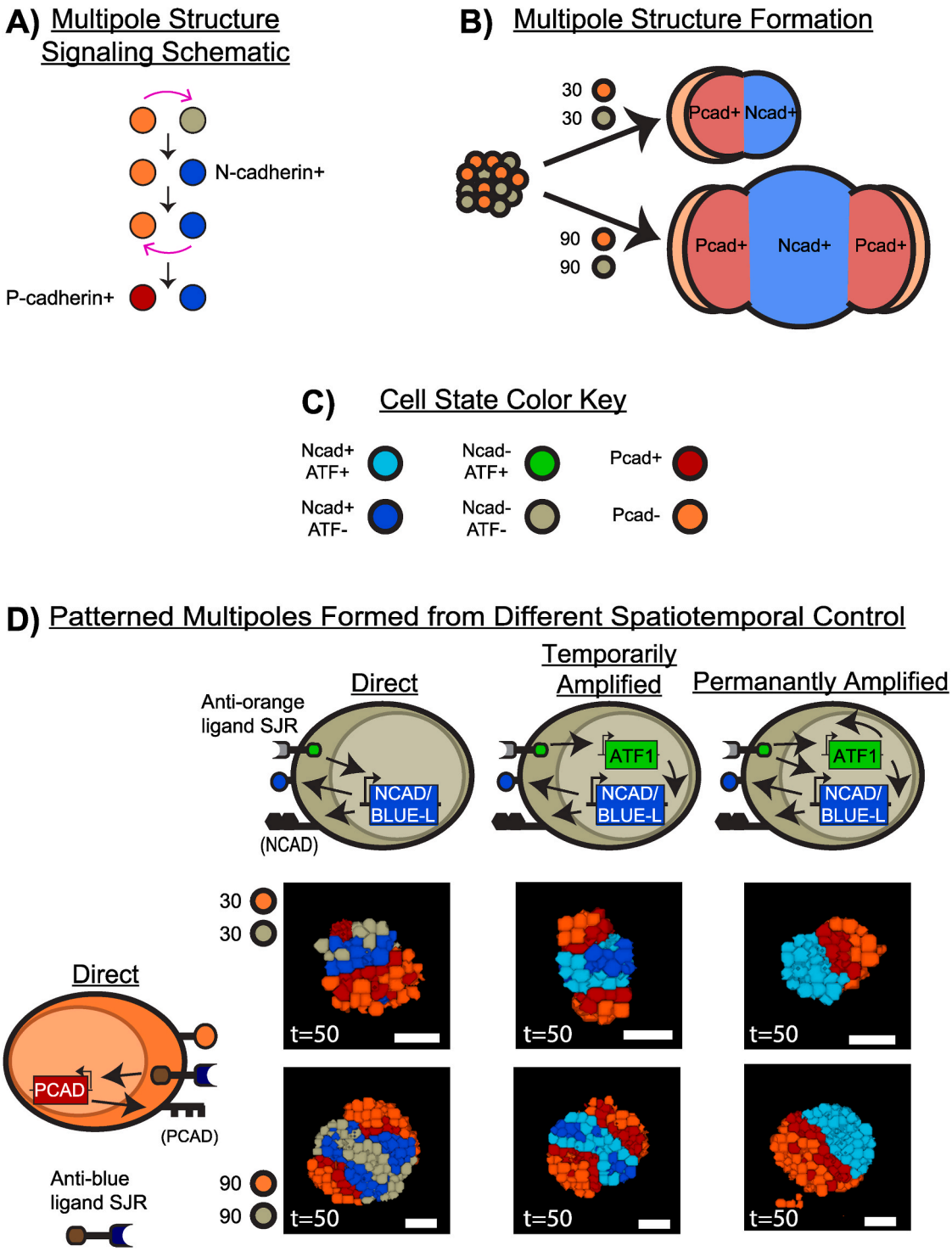

Fig. 3. Combining Amplifiers with SJRs Creates SJR Amplifier Circuits That Enable Spatiotemporal Patterning. A) SJR amplifier circuits were tested for the ability to direct spatiotemporal patterning in a multipole structure. In the original multipole structure schematic, orange cells signal to gray cells turning them blue N-cadherin^{+}. Blue N-cadherin^{+} cells express a ligand enabling them to signal back to orange cells, turning them into red P-cadherin^{+} cells. B) N-cadherin and P-cadherin are homotypically adhesive [9,35], thus mixing orange and gray cells results in multipole structures. C) Cell state color key is given, describing what color corresponds to the expression state of the cell. Ncad is N-cadherin, Pcad is P-cadherin, ATF is activating transcription factor. D) Different circuit combinations and a cross section of the resulting multipole structure. Orange cells always have the direct activation circuit, with P-cadherin (gene is *PCAD*) expression driven by an anti-(blue ligand) SJR. Gray cells have different activation circuits; the anti-(orange ligand) SJR either drives N-cadherin and blue ligand (gene is *NCAD/BLUE-L*) expression directly (Direct Activation) or an amplifier (Temporarily Amplified or Permanently Amplified) that then drives N-cadherin and blue ligand expression. Combining these orange and gray cells demonstrates that different amplifiers enable different temporal control that dictates spatiotemporal patterning. Directly activated gray cells characteristically form a blue stripe with a gray core/pole. Temporarily amplified activated gray cells amplify and prolong N-cadherin expression to form a cyan stripe with a blue core/pole. Permanently amplified activated gray cells permanently amplify and prolong N-cadherin expression to form cyan cores/poles. Mixtures are of 27.4 ± 1.04 orange cells with 29.6 ± 1.04 gray cells or 87.4 ± 1.47 orange cells with 91.6 ± 1.47 gray cells. N = 10 for each circuit combination with one representative cross section shown. Simulations run for 50,000 timesteps. Additional cross sections are given in SFig.3.

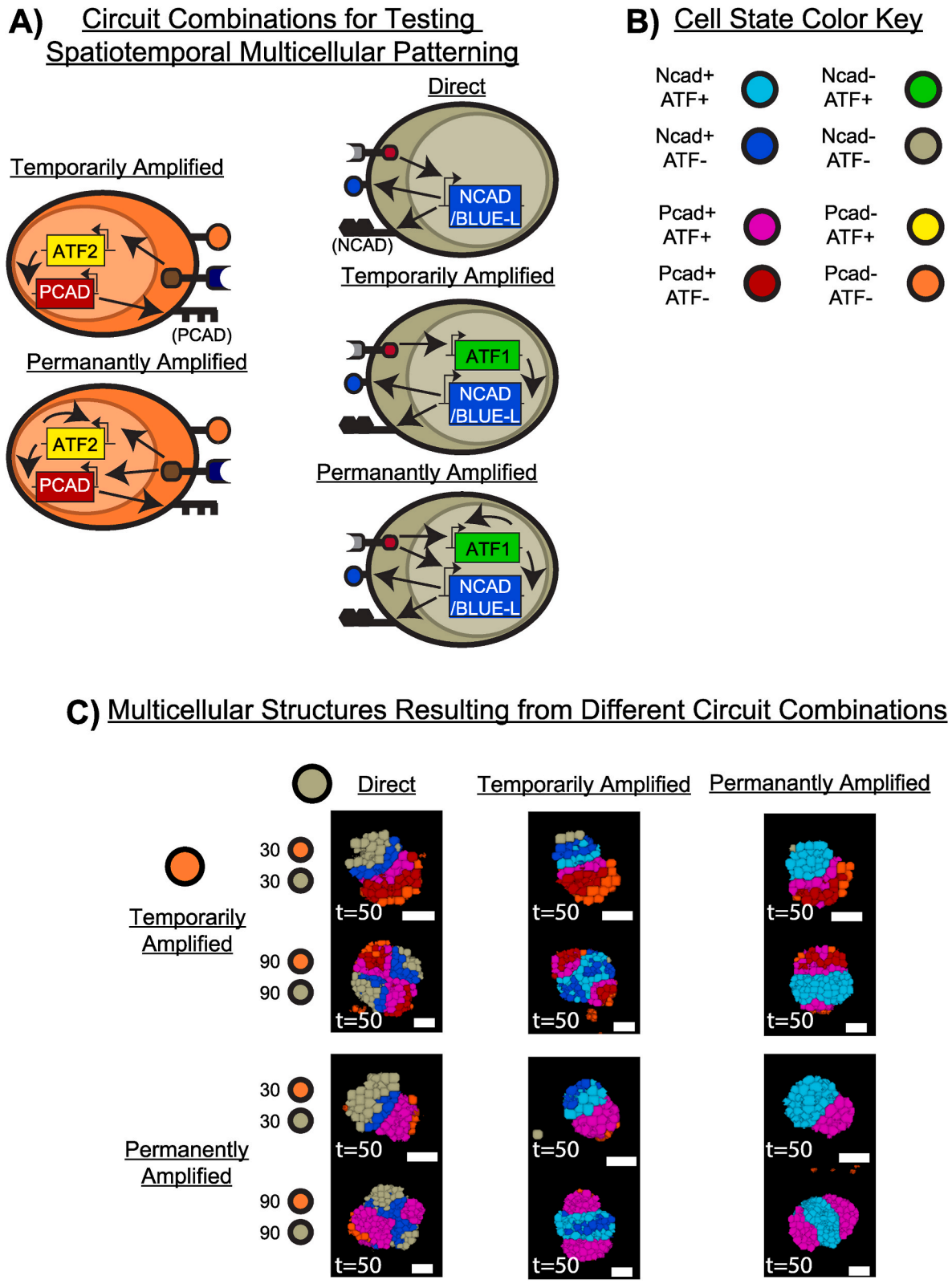

Fig. 4. SJR Amplifier Circuits can be Intercellularly Combined to Create a Variety of Spatiotemporal Structures. A) Orange cells were programmed with either the temporarily amplified activation or permanently amplified activation circuit, then mixed with differently activated gray cells to determine what spatiotemporal patterns could be obtained. B) Cell state color key is given, describing what color corresponds to the expression state of the cell. Ncad is N-cadherin, Pcad is P-cadherin and ATF is activating transcription factor. C) Different circuit combinations and a cross section of the resulting multipole structure. Temporarily amplified activated orange cells consistently formed a pink, red, and orange striped core/pole. Permanently amplified activated orange cells consistently formed a pink core/pole. These patterns could be combined with differently activated gray cells to further expand the patterned multipole structures obtainable. N = 10 for each circuit combination with one representative cross section shown for each initial cell amount. Simulations run for 50,000 timesteps. Additional cross sections are given in SFig.4.

Permanently amplified activated orange cells further expanded the spatiotemporal patterns obtainable, allowing multipole structures with a non-layered pink pole. When combined with directly activated gray cells, they allowed forming a blue stripe with a gray pole and pink pole multipole structure (Fig. 4C). Combining them with temporarily amplified activated gray cells allowed instead a cyan stripe with a blue pole and pink pole multipole structure (Fig. 4C). With the permanently amplified activated gray cells, a cyan, pink pole structure was obtained (Fig. 4C). Additional representative structures of all circuit combinations are given in SFig.4.

2.5. Amplifiers can be used to improve synthetic self-organization

Having shown that the amplifiers, when combined with SJRs, can be used to create SJR amplifier circuits that can direct and expand spatiotemporal multicellular patterning, I next investigated if the amplifiers could be used to improve pattern formation. In the same reference study [9], another structure, the 3-layered structure, was investigated for its robustness of pattern formation. I therefore tested if the amplifier circuits could improve the self-organization of the 3-layered structure.

I used the developmental trajectory in the original study [9]. The 3-layered structure's signaling steps are similar to those in the multipole structure, but the signaling instead drives the expression of two different levels of the adhesion protein E-cadherin. Gray cells receive signal from orange cells and become high E-cadherin positive (blue/cyan colored cells) (Fig. 5A). These high E-cadherin cells form a core and signal back to orange cells, turning orange cells low E-cadherin positive (red colored). End result is a 3-layered structure with a high E-cadherin blue/cyan core surrounded by a low E-cadherin red ring which is surrounded by unactivated orange cells (Fig. 5A). The color key to the cell's state is given in Fig. 5B. Ecad is E-cadherin and ATF is activating transcription factor.

In the original direct activation circuit, cell-cell signaling is achieved via SJRs [9]. Gray cells express an SJR that, in response to orange ligand on orange cells, induces high E-cadherin (gene is *H.ECAD*) along with blue ligand (gene is *BLUE-L*) expression (Fig. 5C). With blue ligand on their surface, gray cells turn blue and signal to orange cells as orange cells constitutively have anti-(blue ligand) SJR on their surface. This induces low E-cadherin (gene is *L.ECAD*), turning orange cells red (Fig. 5C). However, despite using a favorable ratio (~120 gray–~120 orange) and making high E-cadherin and blue ligand easy to express (β Adhesion/Ligand = 1000), this direct activation circuit consistently (5/5) resulted in poor 3-layered structure formation (Fig. 5C). Although the red ring and orange ring were obtained, the desired high E-cadherin core was consistently marred by E-cadherin$^-$ gray cells.

Quantifying core quality with a homogeneity index [35] that measures high E-cadherin$^+$ cell connectedness (i.e. high E-cadherin$^+$ cells contact to other high E-cadherin$^+$ cells, see Homogeneity Index in the Methods Section or the original study [35] for more details), confirmed this observation; core quality saturated around ~0.7 while similar reference structures typically exceed 0.8 (Core Quality, SFig.5A) [35]. This was not due to gray cells being unable to become high E-cadherin$^+$ blue cells. The majority of gray cells became blue as shown by the developmental trajectory and the relative activation plot, but they revert to gray cells as time passed (Developmental Trajectory and Relative Activation, SFig.5A). This is consistent with SJR direct activation to be minimally amplificatory and highly contact dependent [16,19]. Challenging these cells with different ratios that used less orange cells resulted in even poorer structure formation, again off target from the targeted 3-layer structure (Different Ratios, SFig.5A). Similarly poor 3-layered structures formed with the tested ratios at a higher high E-cadherin and blue ligand expression difficulty (β Adhesion/Ligand = 3000, data not shown). An extensive parameter scan of both high E-cadherin/blue ligand expression difficulty (β) and their decay/saturation parameter (κ) confirmed that both qualitatively and quantitatively the direct activation circuit results in poor 3-layered structure formation (SFig.6A).

Using the temporarily amplified activation circuit instead strongly improved target structure formation, consistently yielding 3-layered structure formation in all 5/5 replicates (Fig. 5D). An example developmental trajectory is given in SFig.5B. Although the core was a mix of blue (high E-cadherin$^+$ ATF$^-$) and cyan (high E-cadherin$^+$ ATF$^+$) cells, it consisted of all high E-cadherin$^+$ cells as desired, indicating that high E-cadherin expression was prolonged as is expected of this circuit (Fig. 5D). Moreover, more gray cells became blue/cyan (high E-cadherin$^+$) compared to the direct activation circuit, indicating high E-cadherin expression was amplified as expected (Relative Activation, SFig.5B). Core quality exceeded that in the direct activation circuit and is similar to the values of other quality 3-layered structures (Core Quality, SFig.5B) [35]. Furthermore, at ratios with less orange cells, gray cells with the temporarily amplified activation circuit still managed to become high E-cadherin$^+$ (blue or cyan), allowing target core formation as desired. However, at these ratios the red and orange ring became diminished as is observed *in vitro* (Different Ratios, SFig.3B) [9]. Similar structures were obtained with the tested ratios with β Adhesion/Ligand = 3000 (data not shown). The same extensive scan of both high E-cadherin/blue ligand expression difficulty (β) and their decay/-saturation parameter (κ) confirmed that the temporarily amplified activation circuit, in general, improves 3-layered structure formation (SFig.6B). However, as expression difficulty of high E-cadherin/blue ligand increased, high E-cadherin/blue ligand expression was further delayed, decreasing the quality of core formation (SFig.6B).

Using the permanently amplified activation circuit also improved 3-layered formation, yielding robust 3-layered structure formation (5/5 replicates) with cores of cyan (high E-cadherin$^+$ ATF$^+$) cells (Fig. 5E). Core quality reflected this, exceeding 0.8 (Core Quality, SFig.5C). Compared to the direct activation circuit, more cells became high E-cadherin$^+$ and none reverted from being high E-cadherin$^+$ (Relative Activation, SFig.5C). These results indicate that high E-cadherin expression was both amplified and prolonged as is expected of this circuit. Given that the temporarily amplified activation circuit was able to yield high E-cadherin$^+$ (blue or cyan) cores when challenged with lower orange cell ratios, it is unsurprising that this circuit was also able to yield high E-cadherin$^+$ target cores (Different Ratios, SFig.5C). Developmental trajectory is given in SFig.5C. Similar structures were obtained with the tested ratios with β Adhesion/Ligand = 3000 (data not shown). Extensively scanning both high E-cadherin/blue ligand expression difficulty (β) and their decay parameter (κ) revealed that the permanently amplified activation circuit strongly improves 3-layered structure formation, with core quality exceeding 0.8 at all tested parameters (SFig.6C). While core formation was delayed as expected with increasing expression difficulty, the delay was sufficiently small to nonetheless permit quality core formation (SFig.5C) unlike with the temporarily amplified activation circuit.

These data indicate that the amplifiers are able to improve self-organization; amplifying and prolonging high E-cadherin/blue ligand expression robustly improved target 3-layered structure formation. Different amplifiers also confer different levels of improvement to self-organization. The temporarily amplified activation circuit had decreased 3-layered structure formation at expression difficulties greater than 11000 due to delayed core formation (SFig.6B) while the permanently amplified circuit yielded high quality 3-layered structures at all tested parameters (SFig.6C). As was shown in Fig. 2, these results confirm that circuit behavior is dependent on circuit parameters like decay and expression difficulty.

2.6. Amplifiers improve CAR T cell tumor killing against heterogenous antigen expression tumors

With evidence that the amplifiers amplify and enable temporal control over gene expression, and when combined with SJRs, yield circuits that enable spatiotemporal patterning and improve self-organization in synthetic development, I moved to another synthetic

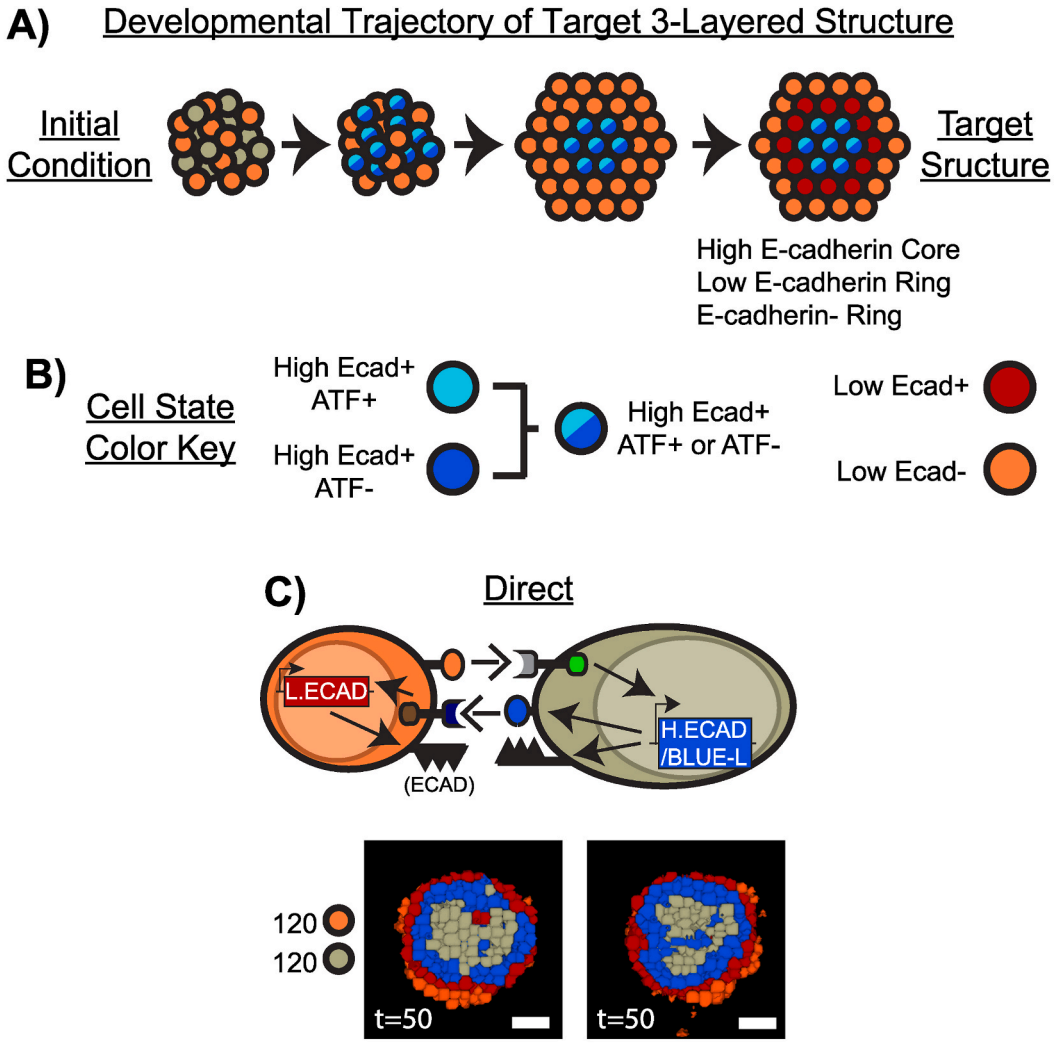

(caption on next page)

Fig. 5. Amplifiers Improve 3-Layered Structure Formation. A) Amplifiers were tested if their amplification and extension of gene expression duration could improve 3-layered structure formation. In the original 3-layered structure developmental trajectory [9], a mixture of gray and orange cells is seeded. Orange cells signal to gray cells and turn them high E-cadherin$^+$ (blue or cyan). These blue/cyan cells express a ligand that signals back to orange cells to turn them low E-cadherin$^+$ (red). This should result in a 3-layered structure with a blue/cyan core followed by a red ring followed by an orange ring. B) Cell state color key is given, describing what color corresponds to the expression state of the cell. Ecad is E-cadherin and ATF is activating transcription factor. C) Representative cross sections of two 3-layered structures formed from directly activated orange cells and gray cells. Circuits are given. Anti-(orange ligand) SJR on gray cells directly drives high E-cadherin and blue ligand expression but consistently results in poor structure formation with the core marred by high E-cadherin$^-$ gray cells. D) Cross sections of two 3-layered structures formed from directly activated orange cells and temporarily amplified activated gray cells. The amplifier driving high E-cadherin and blue ligand expression robustly improves 3-layered structure formation, yielding a mixed blue and cyan core of high E-cadherin$^+$ cells. E) Permanently amplified activated gray cells also strongly improve 3-layered structure formation but yields a completely cyan core instead. Mixtures are of 123.8 ± 2.67 orange cells and 127.2 ± 2.67 gray cells. N = 5 for each with two representative cross sections shown. Simulations run for 50,000 timesteps. Additional structures and results are given in SFig.5 and 6.

biology subfield that heavily relies on SJRs: synthetic immunotherapy [2,15–18,21,36,37]. Due to their high spatial control, modularity, and recent humanization, SJRs are rapidly accelerating towards clinical use [2,15–18,21,36,37]. As a result, SJR-based direct activation circuits currently dominate the subfield, enabling programming T cells with novel behaviors such as multi-antigen discrimination (logic gating) [14–16,21,37]. Such behavior in T cells has powerful implications; the tumors targetable can be broadly expanded as there is no longer the need to rely on a single specific antigen [2,3,11,12,15–17,21,39]. These logic-gated synthetic biology (SB) CAR T cells have been deployed *in vivo* with a prime and kill strategy against a heterogenous antigen expression tumor [16,21,37].

In the prime and kill strategy against a heterogenous tumor, SB CAR T cells have an SJR that, in response to tumor antigen one, induces expression of a chimeric antigen receptor (CAR) against tumor antigen two. This direct activation circuit has highly localized anti-tumor effects; SB CAR T cells primed by dual antigen positive tumor cells killed both dual antigen and neighboring single antigen positive tumor cells [21,37]. Killing was spatially restricted to the tumor area and SB CAR T cells required both antigens present to mediate tumor clearance.

Against this tumor, the directly activated SB CAR T cells are highly dependent on the spatial presence of the priming antigen, tumor antigen one, to maintain CAR expression and kill tumor cells [21,37]. I therefore tested if CAR amplification and prolonged duration of expression conferred by the SJR amplifier circuits could improve tumor killing [16]. As the direct activation circuit in SB CAR T cells is effectively the direct activation circuit in the multipole structure and 3-layered structure (Figs. 3–5), but with the CAR replacing the cadherin/blue ligand as the target gene, I could therefore modify the directly activated gray cells from those experiments, along with the amplifier imbued cells, to create a simple but highly modular setup for testing these cells against these tumors.

To target a heterogenous tumor with the prime and kill strategy, I reprogrammed the cadherin expressing gray cells into SB CAR T cells by coding the SJR to respond to yellow tumor antigen one and replacing the cadherin/blue ligand gene with anti-(red tumor antigen two) CAR (*ARA CAR*) (Fig. 6A). Yellow tumor antigen one represents tumor antigen one and red tumor antigen two represents tumor antigen two (Fig. 6C). In directly activated gray SB CAR T cells, the SJR directly drives CAR expression (Fig. 6A) whereas in the amplifier imbued SB CAR T cells (Fig. 6B), the SJR drives the amplifier which then drives CAR expression. I then created the remaining cells with the appropriate antigen combination. Surrounding (S) cells have neither tumor antigen one (yellow antigen) nor tumor antigen two (red antigen) on their surface and they represent normal healthy cells around and within the tumor. Dual antigen (DA) tumor cells have yellow tumor antigen one and red tumor antigen two on their surface. Single antigen tumor cells (U) have the red tumor antigen. Tumor cells can receive pro-apoptotic signals from SB CAR T cell CAR signaling as is *in vitro* [40–42].

Then, by seeding different combinations of these four cell types, I could create a variety of heterogenous tumors. Initial testing with two cell ratios differing primarily in SB CAR T cell number yielded similar results (SFig.7). Temporarily amplified activated (TAA) and permanently amplified activated (PAA) SB CAR T cells had more CAR$^+$ cells than the directly activated (D) cells (SFig.7A). Confirming the amplification and temporal behavior of these circuits, more gray cells became CAR$^+$ and maintained being CAR$^+$ over time (SFig.7B). The direct activation circuit, as expected, had the majority of gray cells become CAR$^+$ but they reverted to CAR$^-$ as time passed (SFig.7B). Cells with either amplifier appeared to kill more tumor cells than the directly activated SB CAR T cells did (SFig.7C). I validated that these SB CAR T cells required, as is *in vitro* and *in vivo* [21], both antigens to kill tumors cells (SFig.8).

These results indicate that amplifier imbued SB CAR T cells can improve heterogeneous tumor killing compared to the directly activated cells, but this advantage is moderate. The tumor survival difference was ~10 % and overall, all circuits had potent tumor killing (SFig.7C). In these trial experiments, I had kept the amount of tumor cells relatively fixed, varying the SB CAR T cell numbers. I therefore decided to challenge the SB CAR T cells to kill a variety of tumors with different ratios of tumor cell types, dual antigen tumors cells (DA) to single antigen tumor cells (U), a mixture that is commonly performed *in vitro* [21] (Fig. 6C).

At lower DA:U ratios, where there are less tumor antigen one as there are less DA cells, the amplifier imbued cells had more CAR$^+$ cells compared to the directly activated SB CAR T cells (Fig. 6D). Neither amplifier circuit (TAA is temporarily amplified activated and PAA is permanently amplified activated) differed in CAR$^+$ percentage (Fig. 6D). Reflecting this, both circuits outperformed the direct activation circuit, significantly killing more tumor cells with no significant difference between one another (Fig. 6E). At the lowest DA:U ratio, directly activated cells did not even differ from the control cells (SB CAR T cells without the circuit, analogous to untransduced primary T cells) in tumor killing (Fig. 6E). However, as the ratio of DA:U increased, more tumor antigen one became available and decreased these differences, resulting in both CAR$^+$ percentage and tumor cell killing converging across all circuits (Fig. 6D and E). These results indicate that when targeting a heterogenous tumor with low levels of tumor antigen one (the priming antigen), using an amplifier could yield superior tumor killing compared to using directly activated cells.

2.7. Amplifiers improve CAR T cell tumor killing against heterogenous tumors across various challenging conditions

In both the trial experiments (SFig.7) and the various heterogenous tumor experiments (Fig. 6), I had used the optimal parameters for SB CAR T cell performance: CAR expression was very easy (expression difficulty, $\beta_{CAR} = 1000$), CAR surface saturation levels high (maximum CAR surface level, $\kappa = 25000$), tumor cells were very easy to kill (pro-apoptotic protein expression difficulty as a result of CAR signaling, $\beta_{apoptosis} = 1000$), and priming antigen levels high on the corresponding cells ($L = 10000$). To further examine where the amplifier circuits would confer a potent advantage to SB CAR T cell tumor killing, I subjected the SB CAR T cells to a gauntlet of challenges based on these parameters (Fig. 7).

For these challenging heterogenous tumors, I incorporated healthy surrounding (S) cells to better model an *in vivo* tumor setup [16,17,21,

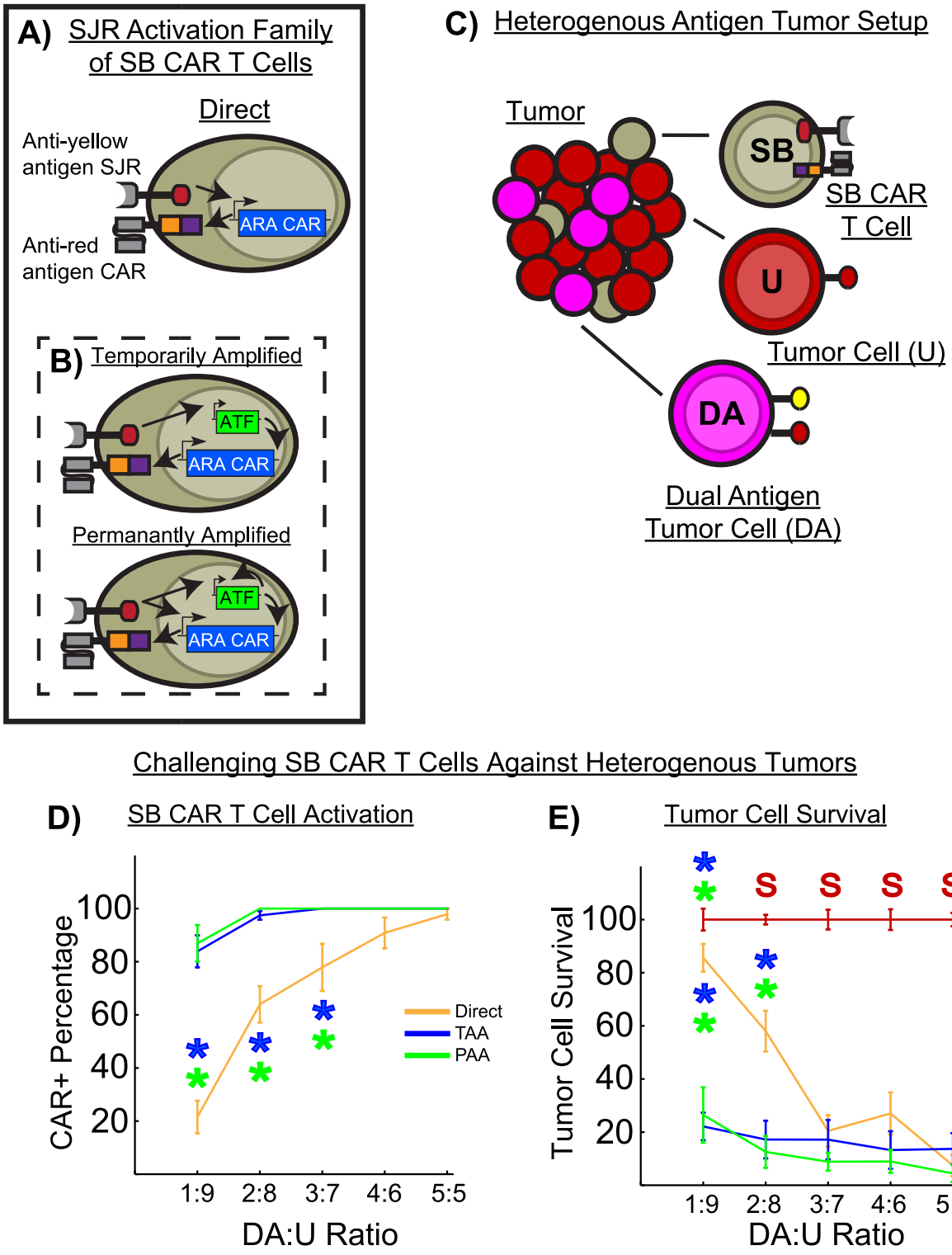

Fig. 6. SJR Amplifier Circuits Improve CAR T Cell Killing Against Various Heterogenous Tumors. A) Activation family of SB CAR T cells created by rewiring the cells used in the 3-layered and multipole structures. The SJR is rewired to sense yellow antigen and the cadherin/blue ligand target gene is replaced with anti-(red antigen) CAR (*ARA CAR*). In the direct activation circuit, the SJR directly drives expression of ARA CAR. *In vitro*, these cells have highly localized anti-tumor effects and require both antigens to activate and kill tumor cells [21,37]. B) In the amplifier imbued SB CAR T cells, the SJR drives an amplifier that then drives the ARA CAR. C) Creation of the various heterogenous tumors with different dual antigen (DA) to tumor (U) ratio. Tumor consisted of a mix of SB CAR T cells, DA cells, and U cells with DA:U ratio specified per experiment. Pink dual antigen (DA) cells have yellow tumor antigen one and red tumor antigen two. Red tumor (U) cells have red tumor antigen two. Heterogeneous tumors are approximately 15 SB CAR T cells with a combined total of around 160 DA + U cells. D) SB CAR T cell activation in different DA:U ratio tumors. SB CAR T cells with an amplifier overall had more CAR^+ cells compared to directly activated cells, especially at lower DA:U ratios. Circuit and curve color key is given in the plot. E) Tumor survival in different DA:U ratio tumors. Amplifiers overall allowed killing more tumor cells at lower DA:U ratios. N = 5 for each circuit for each parameter tested. * denotes significant difference and is colored the curve it differs from. S denotes significant difference from all three circuits. Simulations run for 50,000 timesteps with shown data from this endpoint.

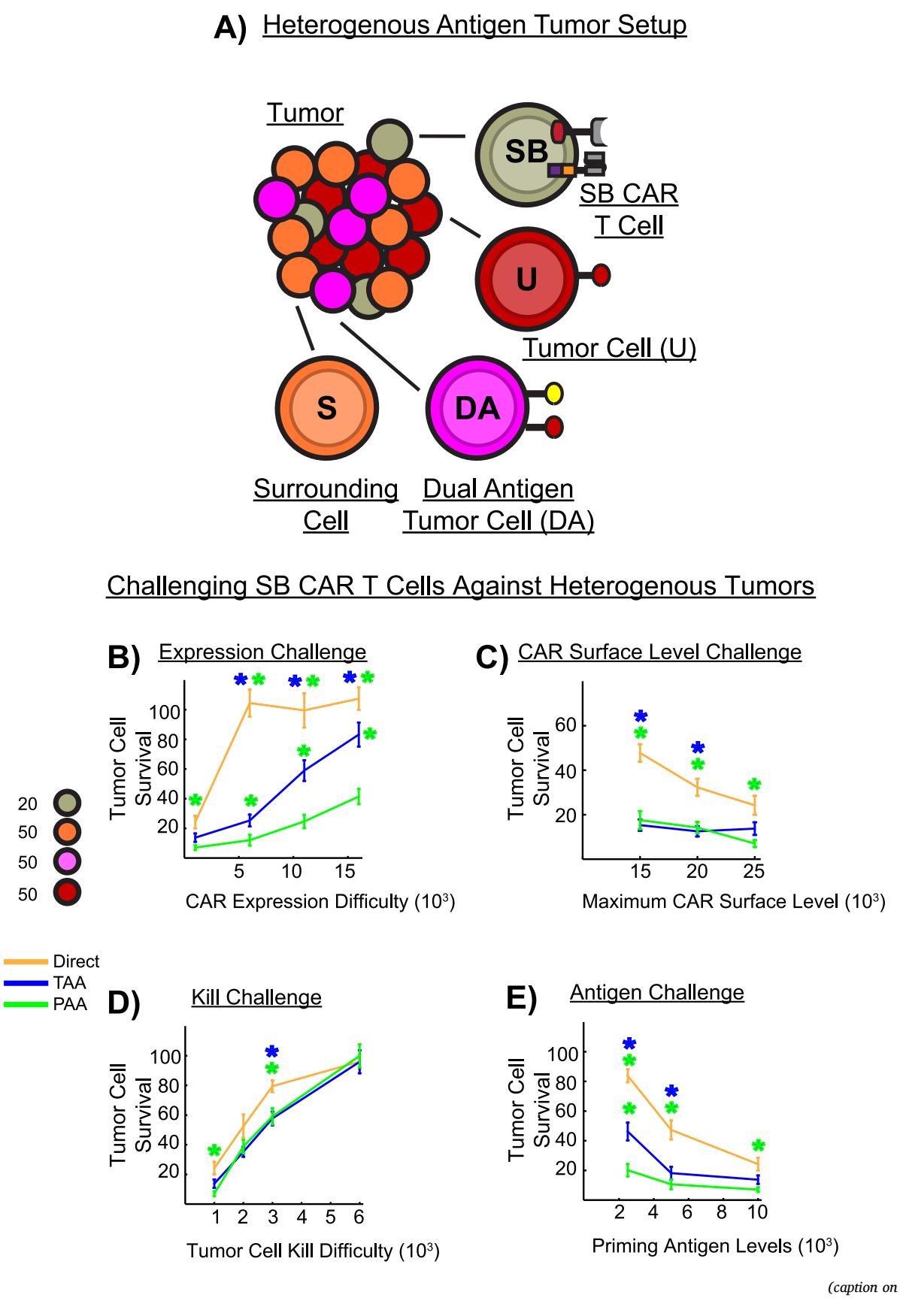

(caption on next page)

Fig. 7. SJR Amplifier Circuits Improve CAR T Cell Killing Against Heterogenous Tumors Across a Variety of Conditions. A) Creation of the heterogenous antigen tumor setup. These cells were tested against a heterogenous tumor *in vivo* [21] and to mimic this, I created the cells necessary to make an *in silico* model of this tumor. Orange surrounding S cells have no surface antigen and represent surrounding healthy cells. Pink dual antigen (DA) cells have yellow tumor antigen one and red tumor antigen two. Red tumor (U) cells have red tumor antigen two. Mixing these cells with the gray SB CAR T cells enables creating a variety of heterogenous tumors. Heterogeneous tumor here is 19.8 ± 0.85 gray SB CAR T cells with 55.7 ± 2.13 orange S cells with 52.5 ± 2.33 red U cells and 51 ± 1.82 pink DA cells. Circuit and curve color key is given to the left of the bottom plots. B) CAR Expression Challenge. SB CAR T cells were challenged with increasing difficulty of CAR expression (β CAR) and relative tumor cell survival quantified. Overall, using an amplifier to amplify and prolong CAR expression decreased tumor cell survival more than the direct activation circuit did. C) CAR Surface Level Challenge. SB CAR T cells were challenged with different maximum CAR surface levels (κ) and tumor cell survival quantified. At lower maximum CAR surface levels, SB CAR T cells with amplifiers decreased tumor cell survival more than the directly activated cells did. D) Kill Challenge. SB CAR T cells were challenged to kill increasingly CAR signaling resistant tumor cells. Amplifier imbued SB CAR T cells moderately decreased tumor cell survival more than the direct activated cells did, indicating that amplifying and prolonging CAR expression could aid in removing CAR signaling resistant tumors cells. E) Antigen Challenge. SB CAR T cells were challenged to kill lower antigen tumor cells. Amplifier imbued SB CAR T cells could amplify the smaller signal and kill more tumor cells. N = 10 for each circuit for each parameter tested. * denotes significant difference and is colored the curve it differs from. Simulations run for 50,000 timesteps with shown data from this endpoint.

37] (Fig. 7A). I began with a common challenge in engineering synthetic circuits. Sufficient expression of the induced target gene is often difficult, typically requiring several iterations of the construct to achieve the desired behavior [43–45]. I therefore challenged these SB CAR T cells by increasing the expression difficulty of the CAR via increasing the parameter β CAR (Expression Challenge, Fig. 7B). At the easiest expression difficulty (β CAR = 1000), both the temporarily amplified activated (TAA) and directly activated (D) SB CAR T cells had similar performance, but the latter quickly lost tumor killing capabilities as CAR expression difficulty increased (Fig. 7B). Temporarily amplified activated SB CAR T cells decreased tumor cell survival more than the directly activated cells did at higher difficulties (Fig. 7B). Permanently amplified activated (PAA) SB CAR T cells managed to maintain superior tumor killing over the other circuits as expression difficulty increased (Fig. 7B). These results indicate that when targeting a heterogenous tumor, if CAR expression difficulty is a concern, using an amplifier to amplify and prolong CAR expression could improve tumor killing. Furthermore, using the permanently amplified activation circuit could be additionally advantageous to using the temporarily amplified activation circuit.

Alternatively, CAR T cell anti-tumor capabilities can be impaired by insufficient surface levels of CARs [46–48]. To determine how this affects amplifier imbued SB CAR T cells, I challenged the cells by testing different CAR surface saturation levels, modelled by parameter κ in GJSM (CAR Surface Level Challenge, Fig. 7C). Expression of CAR was kept easiest (β CAR = 1000) and overall, both amplifier circuits outperformed the direct activation circuit (Fig. 7C). These results indicate that against a heterogenous tumor, when CAR surface levels saturate low, amplifier circuits can yield superior tumor cell killing.

The two above challenges stem from SB CAR T cell engineering, but the tumor cells themselves can hinder killing [42,49–56]. Tumor cells can resist CAR T cell mediated apoptosis via alteration to the death receptor pathways [40–42]. This can be modelled in my setup by increasing the parameter β apoptosis, which models pro-apoptotic protein expression as a result of CAR signaling (Kill Challenge, Fig. 7D). The amplifier circuits overall appeared to decrease tumor cell survival more than the direct activation circuit, but the difference was moderate, ranging from 10% to 20 % (Fig. 7D). As kill difficulty increased, tumor cell survival increased as expected (Fig. 7D). These data indicate that when tumor cells become more resistant to CAR T cell cytotoxicity, amplifying and prolonging CAR expression could confer a moderate advantage.

In an alternative but common mechanism, tumor cells can evade CAR T cells by downregulating tumor antigen expression [17,50–52,54,55]. I therefore tested the SB CAR T cells against tumors with varying levels of yellow tumor antigen one. At the lowest antigen level (L = 2500), amplifier imbued SB CAR T cells decreased tumor cell survival more than the directly activated cells did, with the permanently amplified activated cells further outperforming the temporarily amplified activated cells (Fig. 7E). As the antigen level increased, performance difference between all three diminished but permanently amplified activated cells maintained significantly decreased tumor survival compared to the directly activated cells (Fig. 7E). Thus, amplifying and prolonging CAR expression can improve tumor killing where there is tumor antigen downregulation. At low antigen levels, the permanently amplified activation circuit can yield superior tumor killing compared to the other two circuits.

3. Discussion

Amplifiers that amplify target gene expression and enable unidirectional temporal regulation expand the control of the circuits commonly used in synthetic development and synthetic immunotherapy. Here I show via mathematical and *in silico* analysis that the activating amplifiers amplify target gene expression and enable prolonging duration of target gene expression, with different amplifiers enabling differing levels of temporal control. In synthetic development, amplifiers combined with SJRs enable spatiotemporal patterning and improve target structure formation. In synthetic immunotherapy, these amplifier circuits can improve synthetic biology (SB) CAR T cell tumor killing against various heterogenous antigen expressing tumors. Together, these results demonstrate the capabilities and potential use of amplifiers in not just basic applications, but also clinical applications as well.

To study the capabilities and applications of these SJR amplifier circuits, I used GJSM implemented in a cellular Potts model [26,34,35]. This model combination has been previously validated for predicting self-organization and patterning driven by SJRs [35]. The two synthetic development structures (multipole and 3-layered) that have been further examined in this study were originally modelled *in silico* by this model combination [35]. Although this framework was not previously validated for synthetic immunotherapy, the setup I created to model SB CAR T cells and the tumors yielded results similar to those obtained biologically [21,37]. Directly activated *in silico* SB CAR T cells strongly killed tumor cells (SFig.7) as is observed *in vitro* [21]. These *in silico* cells were highly dependent on SJR signaling to become CAR^+ (SFig.8) and maintain being CAR^+ (killing of DA cells resulted in reversion to CAR^-, SFig.7). These are all features observed *in vitro* [21]. Therefore, while numerous factors remain to be included and refined (i.e. cytokine secretion and signaling, T cell activation mediated expansion, exhaustion, etc), this simple setup provides a viable platform for computationally testing a variety of SB CAR T cells against a variety of tumors. Developing this platform could expand *in silico* methods in synthetic immunotherapy and create a pipeline similar to how GJSM is currently used to test circuit designs for synthetic development [35]. While computational efforts for synthetic immunotherapy begin with this study, similar efforts are at least underway for regular CAR T cell immunotherapy [57–61].

An additional advantage of using a mathematical and *in silico* approach is that it enabled me to rapidly yet thoroughly investigate the amplifiers and their circuits. Changing parameters (i.e. type of gene expressed, expression difficulty, surface saturation levels) was simply changing code while reengineering cells *in vitro* would likely take years

with one researcher as in this study. However, using a computational approach does give a theoretical analysis of the circuits. For example, transcription factor feedback loops similar to those in the permanently amplified activation circuit (Fig. 1F) do not always maintain permanent gene expression *in vitro* [32,62–65]. Some cells can lose permanent gene expression over the course of multiple generations, and this is hypothesized to be a combination of epigenetic silencing and/or failure of daughter cells receiving sufficient transcription factors post mitotic division [32]. Insufficiency of transcription factor prevents positive regulation, reverting cells to the non-amplified state, highlighting that amplifier behavior depends on not just circuit design but also circuit parameters. Depending on the purpose of the circuit, this feature may be desirable. Permanently amplified activated SB CAR T cells increase tumor cell killing but theoretically can increase the risk of on-target off-tissue toxicity. Loss of CAR expression can mitigate this and continued expression of the SJR allows these cells to spatially reactivate where they are again exposed to the tumor. If undesirable, this limitation could be overcome by increasing transcription factor levels before division [32,63] or reactivating silenced genes through another synthetic circuit [66,67].

In this study, I designed the circuits generically (i.e. ATF1, anti-yellow antigen SJR, etc) such that there is no specific SJR (i.e. anti-CD19 synNotch) or specific transcription factor (i.e. LexA-VP64) modelled. I have left it to the user to choose the specific components for the circuits but there are several design subtleties to note. First, I have deliberately designed these circuits with avoidance of hybrid combinatorial promoters as they have been shown to function with synergistic effects not tested with the GJSM model [68]. The results here are unlikely to be predicative if the user chooses to deploy hybrid combinatorial promoters with the amplifiers. Second, there are concerns that with the amplifiers, the ATF levels can fluctuate between high and low states in single cells due to stochastic effects. While this is possible, it has yet to be observed in synthetic transcription factor feedback loops [32,69].

Circuit generalizability should additionally extend amplifier compatibility beyond SJRs to other transcription factor based receptors as well. As the amplifiers are transcription factor based, they should be compatible with other transcription factor based receptors such as modular extracellular sensor architecture (MESA), double-cut transcription activation receptor (DocTAR), and Tango/ChaCha [68–77]. MESA/DocTAR are fully modular synthetic receptors that dimerize in response a choice soluble ligand to release a choice transcription factor [68,69,73,74,77] while Tango/ChaCha are modified GPCRs that bind a soluble ligand to release a choice transcription factor [72,76]. Then, having these receptors release a transcription factor that drives the amplifier, rather than the target gene, should enable amplification and prolongation of target gene expression as is observed with SJRs. In theory, these amplifiers should be broadly compatible with transcription factor based circuits overall. In fact, a proof-of-concept has recently emerged supporting amplifiers and this compatibility hypothesis; the DocTAR receptor is compatible with a simple amplifier [69].

The amplifiers and SJR amplifier circuits designed in this study serve as generic yet flexible tools for improving control in synthetic biology. While simple in concept, the ability to add gene amplification and prolong duration of gene expression broadly expands the capability of SJR based circuits and likely other transcription factor based circuits as well. Though the experiments here focused on adhesion-based self-organization and T cell immunotherapy, combining these amplifiers with different synthetic receptors, in principle, broadly expands control over processes such as tissue regeneration [19] or other immune cell behavior [78,79]. As an independent investigator without resources, funding, and a lab, I was unable to perform the biological versions of the simulations. This work supports future studies to explore and test the capabilities of these amplifiers and SJR amplifier circuits in biological experiments, hopefully promoting the use of amplifiers in synthetic circuits. In an upcoming accompanying paper, I demonstrate mathematically the ability of these amplifiers to drive other amplifiers and obtain inhibitory gene expression that shortens duration of or turns off gene expression.

4. Methods

4.1. Key resource table

REAGENT or RESOURCE	SOURCE	IDENTIFIER
Software and Algorithms		
CompuCell3D (CC3D) v3.7.8	[34]	RRID: SCR_003052
Mathematica v12.0.0.0	Wolfram Research	RRID: SCR_014448
JMP v11.0.0	SAS Institute	RRID: SCR_014242
Excel v2301	Microsoft	RRID: SCR_016137
General Juxtacrine Signaling Model (GJSM) in CC3D	[35]	N/A

4.2. Lead contact

Requests for information, resources, and code will be fulfilled by Calvin Lam (calvin.lam.k@gmail). Example and template codes for the simulations here can be found at: https://github.com/calvinlamk/Activating-Amplifiers/tree/main.

4.3. The in silico cell line ISL929 in CompuCell3D

ISL929 is an *in silico* cell line developed in the cellular Potts modeling software CompuCell3D (CC3D) and has been previously combined with the Generalized Juxtacrine Signaling Model (GJSM) to successfully predict synthetic juxtacrine receptor (SJR) driven self-organization [34,35]. As ISL929 is specifically designed to model the *in vitro* mouse fibroblast cell line L929 used in the reference biological self-organization experiments (3-layered and multipole) [9], I chose to use ISL929 as my *in silico* cell line. I provide a brief description of ISL929 below and the original *in silico* study that developed this line is given here [35].

ISL929 is implemented in CC3D as 3D multipixel cells that have physical properties such as surface area, volume, adhesion, and motility. ISL929 cells are programmed to desire a spherical morphology as is observed in suspension *in vitro* [9,35]. Each cell (σ) is assigned a desired radius (DR) drawn from a Gaussian distribution with mean of 3 pixels and standard deviation 0.5 pixels. The desired surface area (DS) and desired volume (DV) are then calculated from this desired radius ($4\pi r^2$ for surface area and $4/3\pi r^3$ for volume), promoting cells to want a spherical morphology. How strongly the cell desires this spherical morphology is determined by the parameters λ_S for the desired surface area and λ_V for the desired volume. These parameters can be thought of as the spring constants in Newtonian physics. Then, a population of ISL929 is relatively homogenous in morphology, overall consisting of spherical cells but with slight size differences due to differing in desired radius. For ISL929, λ_S and λ_V are set to 2.2, generating cells that are spherical as is observed with *in vitro* L929 cells [9,35]. However, if ISL929 cells are modified with different circuits that change adhesion, these parameters can change as determined in both the *in vitro* and *in silico* study [9,35]. Full parameters are given in Supplementary Table 1.

With the basic morphology of ISL929 cells defined, growth and division can be implemented. Growth is achieved by subjecting the desired radius DR to fluctuations drawn from a uniform distribution, with a slight skew towards increasing the desired radius ($-3*10^{-3.88}$ to $4*10^{-3.88}$). Cells therefore slowly increase their desired radius, increasing the desired surface area and volume as well. When cells reach the threshold volume ($2*4/3\pi r^3$ with $r = 3$ pixels), cells undergo symmetric division into two cells. After division, the parent cell is assigned a

new desired radius and undergoes growth once again. The child cell is assigned the same parameters. With these rules and parameters, ISL929 roughly doubles every 24000 timesteps and as *in vitro* L929 cells roughly double every 24 h, this sets 24000 simulation timesteps to 24 h in real time [9,35].

In vitro L929 cells weakly adhere to one another and in CC3D, cell-cell adhesion is defined by a matrix of parameters J. Cell adhesion to different cells (i.e have cadherin or different cadherin expression) have different J values. However, as *in vitro* L929 weakly adhere and do not express any cadherin, ISL929 have basal adhesion value J = 49 to any other cell type, cadherin expressing or not. This is defined relative to the media such that J = 49 sets ISL929 cells to weakly aggregate to one another in the simulated media. Like with λ_S and λ_V, however, these J values can change as ISL929 cells are modified with different circuits that drive different cadherins [9,35]. Full parameters are given in Supplementary Table 1.

Cell motility in CC3D is defined by parameter T and as strong adhesion (i.e. cadherin expression) is generally abstracted to decrease cell motility [80–82], ISL929 motility is defined by the formula

$$T_\sigma = T_0 + \zeta \sum_k \frac{J_{type(\sigma),k} * total\ contact\ surface\ area\ with\ k}{surface\ area\ (\sigma)}$$

Each cell σ is assigned its own T value according to this formula, with T_0 being basal motility and ζ being the weight of adhesion attenuating motility. The summation term determines the motility of the cell due to the adhesivity of its local environment. K designates the types of cells to sum over, with types of cells stratified by surface expression of cadherins (i.e. one type of cell is high E-cadherin$^+$ while another could be low E-cadherin$^+$). For example, a simulation with high E-cadherin$^+$ ISL929 and low E-cadherin $^+$ ISL929 would have two cells types and thus k sums up to two. $J_{type(\sigma),k}$ is the adhesion value of the type of focal cell σ to cells of type k. For example, if the focal cell is of parental ISL929 type, then its J value is 49 to any other cell type k. This J value is then fractionalized to the total contact surface area with cells of type k by dividing over the focal cell's surface area (surface area (σ)). Higher contact area with less adhesive cell types (higher J value) results in a higher value from the summation term, yielding higher motility. Maximum motility is obtained in the medium, with J = 52 for cell to medium adhesion. Overall, this motility formula allows a cell to sense the adhesivity of its local environment and attenuate its motility accordingly. In general, more adhesive environments lower motility while less adhesive environments restore motility. Parental ISL929 have T_0 set to 100, ζ set to 0.5, and J set to 49, resulting in highly motile cells as is observed *in vitro* [9,35,83]. Full parameters are given in Supplementary Table 1.

With the physical and basic properties of ISL929 defined (all the properties described thus far are identical to those in the original computational study [35]), cell motion can finally be described. Cells move in the cellular Potts model by "pixel copy attempts". That is, cells attempt to move by copying their pixels over to a neighboring pixel [26,34,35]. The success probability of this move is determined by the probability function $P = e^{-\Delta H/T}$, where P is the probability of success, ΔH the change in global system energy calculated from all the pixel copy attempts at said timestep, and T the focal cell motility. As ISL929 has surface area, volume, and adhesion, H takes the form of

$$H = \sum_{i,j} J_{\sigma_i \sigma_j}\left(1 - \delta_{\sigma_i \sigma_j}\right) + \sum_{\sigma} \left(\lambda_S (\sigma_S - \sigma_{DS})^2 + \lambda_V (\sigma_V - \sigma_{DV})^2\right)$$

as in Refs. [26,35]. σi and σj are the identities of cells that occupy pixel site i and j, respectively. $J_{\sigma i\, \sigma j}$ is the adhesion value of the types of cells of σ_i and σ_j. The Kronecker delta (δ) term limits the calculation to cell-cell interfaces. λ_S and λ_V controls the cell's desire to achieve its desired surface area (σ_{DS}) and desired volume (σ_{DV}), respectively. σ_S and σ_V are the cell's actual surface area and volume, respectively, at a given timestep.

4.4. Brief overview of Generalized Juxtacrine Signaling Model (GJSM)

Generalized Juxtacrine Signaling Model (GJSM) is a mathematical model developed and validated to describe synthetic juxtacrine receptor (SJR) regulation of a target gene's expression [35]. SJR activation of target gene expression can be described by the equation

$$\frac{dR}{dt} = \frac{1}{1 + Exp[-(S - \beta)]} - \frac{R}{\kappa}$$

The change in target gene protein level (R) at a given timestep is a balance between production from SJR signaling (first term) and loss from degradation (second term). In the first term, production is calculated from signal (S) and target gene expression difficulty (β). Because SJRs and transcription factors activate expression in this study, S models SJR or transcription factor signaling that drive the amplifier and/or target gene. However, as it is suggested that synthetic transcription factor based circuits are bistable (either sufficient or insufficient transcription factor to drive expression [32,63]), S should be weighed against an expression difficulty parameter β. β models the difficulty of gene expression, encompassing a variety of biological factors such as promoter, transcription, and/or translation inefficiency, or expression delay [35]. The logistic form of the production term (Exp is e) smoothly limits production from 0 to 1 per timestep, representing minimal to maximal production at a given timestep. This equation form was chosen over the Hill form for several reasons as previously described [35]. The parameters S, β, and κ have simple intuitive interpretations and make it easy to design circuits, especially for users new to SJR circuit design. Kinetic interpretations nonetheless remain as the logistic function is a transformed but mathematically equivalent version of the more standard Hill function [84–87].

The degradation term is the standard linear decay rate commonly deployed in biochemistry models. Target gene protein level R decays proportionally to itself and inversely to decay constant κ. κ controls the protein saturation level. For example, in the synthetic development experiments (3-layered and multipole, Figs. 3–5), it can control the maximum level of cadherin and/or blue ligand while in the synthetic immunotherapy experiments (Figs. 6–7), it can control maximum CAR surface level. Then, the degradation term also ranges from 0 to 1 per timestep, representing minimal to maximal degradation at a given timestep.

4.5. The SJR amplifier circuits as modelled by GJSM

With the base equation described, the equations for the activation circuits (direct activation circuit, temporarily amplified activation circuit, permanently amplified activation circuit) can now be defined.

4.5.1. Direct activation circuit

Because the direct activation circuit is the SJR driving target gene expression directly (Fig. 1D), the circuit equation is

$$\frac{dR}{dt} = \frac{1}{1 + Exp[-(S_{SJR} - \beta)]} - \frac{R}{\kappa}$$

This form is identical to those in previous direct activation circuits [35] and parameters are as described in the above section. S_{SJR} is the number of activated SJRs (binding cognate ligand/antigen to release its transcription factor) at a given timestep. See how S_{SJR} is calculated in the below section, Adding ligands, receptors, and the activation circuits into ISL929.

4.5.2. Temporarily amplified activation circuit

In the temporarily amplified activation circuit, the SJR drives the expression of an activating transcription factor (ATF) that then drives expression of the target gene (Fig. 1E). Because this is a two-step process, two equations are required. First, ATF expression driven by the SJR is described as following.

$$\frac{d(ATF)}{dt} = \frac{1}{1 + Exp[-(S_{SJR} - \beta 1)]} - \frac{ATF}{\kappa 1}$$

ATF production is driven by SJR signal S_{SJR}. β1 controls the expression difficulty for the SJR to drive ATF expression while κ1 controls the maximum/saturation level of ATF protein.

As the ATF drives the expression of the target gene, target gene product level (R) is described by the equation

$$\frac{dR}{dt} = \frac{1}{1 + Exp[-(S_{ATF} - \beta 2)]} - \frac{R}{\kappa 2}$$

S_{ATF} is the ATF levels (ATF from the above equation) at a given timestep and drives the expression of the target gene. β2 controls the expression difficulty for the ATF to drive target gene expression while κ2 controls the maximum/saturation level of target gene protein.

4.5.3. Permanently amplified activation circuit

In the permanently amplified activation circuit, the SJR drives the expression of an activating transcription factor (ATF) and the target gene (R). This ATF also drives expression of itself and thus also the target gene R (Fig. 1F). The equations are as following.

$$\frac{d(ATF)}{dt} = \frac{1}{1 + Exp[-((S_{SJR} + S_{ATF}) - \beta 1)]} - \frac{ATF}{\kappa 1}$$

$$\frac{d(R)}{dt} = \frac{1}{1 + Exp[-((S_{SJR} + S_{ATF}) - \beta 2)]} - \frac{R}{\kappa 2}$$

S_{ATF} is the ATF levels (ATF) from solving the first equation.

The parameters tested in this study for all the above equations are given in Supplementary Table 1. It is important to note that within a set of equations representing an activation circuit, the parameters β and κ can differ between equations due to differences in expression difficulty and degradation.

4.6. Adding ligands, receptors, and the activation circuits into ISL929

With ISL929 cells defined and the mathematical equation of the activation circuits described, I could finally implement the equations into the cells to generate the circuit imbued ISL929 for the synthetic development and synthetic immunotherapy experiments (SFig.1A). I then added constitutive ligand expression onto the appropriate cells (i.e. orange ligand expression on orange cells, red antigen on single antigen positive tumor cells). I simplified the time dependent equation from the original *in silico* study [35] and set it to a constant value L on the cell's surface per simulation. Constitutive SJR expression was then added to the appropriate cells (i.e. anti-(blue ligand) SJR on orange cells, anti-(yellow antigen) SJR on gray SB CAR T cells). As there is no evidence of SJR to be limiting in the reference experiments, SJR surface levels was assumed to be in excess and thus not needed for the subsequent calculations [35]. However, if desired, the full formulation of GJSM can easily model this [35]. Parameters for ligand/antigen levels per experiment are given in Supplementary Table 1.

Having defined the constitutive ligand/antigen levels, it becomes possible to calculate the signal from SJR signaling, S_{SJR}. In the most generic form, SJR signaling is dependent on both the ligand/antigen level the focal cell is exposed to and the SJR receptors on the focal cell that can respond to these ligands/antigens. In this study, because SJR levels are assumed to be non-limiting and because SJRs function in a 1:1 stoichiometry with its ligand (one SJR binds one ligand to release one transcription factor) [16,17,19,35], SJR signal S_{SJR} depends only on the amount of ligand/antigen the focal cell is exposed to (SFig.1B). This can be calculated by the equation below.

$$S_{SJR}\sigma = \sum_{SN} surface\ area\ of\ \sigma\ contacting\ SN * \frac{L}{surface\ area\ (SN)}$$

At a given timestep, focal cell σ receives SJR signal $S_{SJR}\sigma$ calculated from the total cognate ligand/antigen level it is exposed to. Signaling neighbor (SN) is a neighboring cell expressing the appropriate cognate ligand (i.e. orange ligand on orange cells cognate to anti-(orange ligand) SJR on a focal gray cell). For a signaling neighbor SN, the amount of cognate ligand/antigen it presents is calculated by multiplying the surface area the focal cell σ is in contact with the signaling neighbor by the ligand density on said signaling neighbor (L/surface area(SN)). For a constitutive ligand, L is defined as a constant value while for a ligand that is a target gene (i.e. blue ligand), L is defined by the value of R. Repeating this calculation over each signaling neighbor sums the cognate ligand/antigen level the focal cell is exposed to at a given timestep and gives $S_{SJR}\sigma$ at that timestep. While not required in this study, cells with multiple SJRs will have several $S_{SJR}\sigma$ calculated depending on the cognate neighbors present at a given timestep.

4.7. Linking target gene expression to behavior

To link target gene expression to the intended behavior (i.e. cadherin expression, ligand expression, CAR expression), I used a discrete state-transition model as in the original study and commonly deployed in computational biology [26,35,88,89]. If target gene protein level R exceeds a threshold (7000 for all simulations here), then the cell gained the feature of the target gene. Cells with blue ligand level that exceeded the threshold became blue and could signal to cells with anti-(blue ligand) SJR. Cells with high E-cadherin levels that exceeded the threshold became highly adhesive (J changed). Cells with CAR levels that exceeded the threshold could target the cognate tumor cells, a bistability feature that is observed *in vitro* [46–48]. Tumor cells, upon accumulating enough pro-apoptotic proteins as a result of SB CAR T cell signaling, irreversibly commit to apoptosis [42,90–95]. Where cells did not irreversibly fate commit (i.e. cadherin expression, ligand expression, CAR expression), falling under this threshold reverted cells, losing the behavior. Full parameters are given in Supplementary Table 1.

An example schematic of the entire signaling process, from constitutive ligand expression to SJR signaling to amplifier expression to target gene expression to resulting behavior change, is given in SFig.1B.

4.8. General simulation conditions

At the start of the simulation, cells were initialized as a 5 × 5 × 5 pixel cube in a 100 × 100 × 100 pixel lattice. Initial configuration and ratio of cells is specified in the appropriate section below. Data was collected every 100 timesteps for analysis.

4.9. Homogeneity index

To quantify the quality of the 3-layered structure's core and the quality of the multipole structure's poles, I used the homogeneity index defined in Ref. [35]. This measure was previously used to quantify self-organization in the simulated reference structures [35]. As the core forms from high E-cadherin$^+$ cells (blue/cyan) and the poles form from either N-cadherin$^+$ cells (blue/cyan) or P-cadherin$^+$ cells (red/pink), I was interested in the contact between cadherin cells to other same cadherin cells. For example, in the 3-layered structure, I was interested in high E-cadherin$^+$ cells contacting other high E-cadherin$^+$ cells while in the multipole structures, I was interested in N-cadherin$^+$ cells contacting other N-cadherin$^+$ cells and P-cadherin$^+$ cells contacting other P-cadherin$^+$ cells. The average connection strength between these cells can be quantified by the formula below.

$$\psi_x = \frac{\sum_{m=1}^{n} \frac{surface\ area\ of\ cell\ \sigma\ \ in\ contact\ with\ cells\ of\ type\ X}{Surface\ Area\ (\sigma)}}{n}$$

For a cadherin type x (i.e. high E-cadherin), this index calculates how well cells of cadherin type x contact one another. At a given timestep, for a focal cell σ of cadherin type x, if it is in contact with cadherin type x neighbors, its total surface area contact with these cadherin type x neighbors is normalized to the surface area of focal cell σ. This measures the relative strength of cadherin type x connection the cell has to cadherin type x cells at that timestep. Repeating this over all cadherin type x cells in contact with type x cadherin cells and normalizing to the number of contributions yields a global average connection strength for the structure. In this study, as cadherin cells sort to one another, the connection strength increases globally, yielding a measure of sorting. However, this measure can be well generalized depending on the need of the experimenter. See Ref. [35] for the full theoretical description and capabilities of this index.

4.10. Cell-cell signaling assay quantifications

A frozen 5 × 5 × 5 pixel cubic gray cell (i.e. static in volume, surface area, and morphology) was seeded with either 0, 1, 3, or 6 orange 5 × 5 × 5 pixel cubic cells such that one face of an orange cell contacted one face of the focal gray cell. This fixed SJR signaling, S_{SJR}, to a constant value (i.e. 0 orange cells had L*0/6 S_{SJR} while 1 orange cell had L*1/6 S_{SJR} with L = 10000 in this study) and allowed analytically validating the activation circuits as well. For the expression difficulties β = 1000, 3000 and 12000, simulations were run for 100000 timesteps with 0, 1, 3, or 6 orange cells deleted at 25000 timesteps. ATF levels were tracked along with red reporter levels. These results were validated by numerically solving the activation circuits in Mathematica via NDSolve, and this enabled generating plots for the additional two expression difficulties shown (β = 6000 and 18000). Full parameters are given in Supplementary Table 1.

4.11. Multipole structure quantifications

A mixture of orange and gray cells carrying the appropriate activation circuit were seeded as a spherical blob at the center of the simulation lattice and simulation run for 50,000 timesteps. Cross section of a 3D structure is shown and scalebar is from the original *in silico* study [35], 17.5 pixels to 100 μm.

4.12. 3-layered structure quantifications

A mixture of orange and gray cells carrying the appropriate activation circuit were seeded as a spherical blob at the center of the simulation lattice and simulation run for 50,000 timesteps. Cross section of a 3D structure is shown and scalebar is from the original *in silico* study [35], 17.5 pixels to 100 μm *in vitro*. Core quality was quantified using the homogeneity index with high E-cadherin$^+$ cells (blue/cyan) to other high E-cadherin$^+$ cells. Relative activation was quantified by dividing the number of cells of the focal type over the total cells of that genotype. The formulas are given here. Cyan curve is E-cadherin$^+$ cyan cells/(gray cells + green cells + blue cells + cyan cells). Blue curve is E-cadherin$^+$ blue cells/(gray cells + green cells + blue cells + cyan cells). Green curve is E-cadherin$^-$ green cells/(gray cells + green cells + blue cells + cyan cells). Gray curve is E-cadherin$^-$ gray cells/(gray cells + green cells + blue cells + cyan cells). Full parameters are given in Supplementary Table 1.

4.13. Targeting heterogenous tumor quantifications

The appropriate mixture of SB CAR T cells, surrounding (S) cells, dual antigen (DA) tumor cells and/or single antigen (U) tumor cells were seeded as a spherical blob at the center of the simulation lattice and simulation run for 50,000 timesteps. Cells were set adhesive to one another (J = 35 for all) to prevent random dispersion. CAR levels were tracked and CAR$^+$ percentage calculated by (CAR$^+$ cyan cells + CAR$^+$ blue cells)/(gray cells + green cells + blue cells + cyan cells). Because orange surrounding (S) cells have the same characteristics as tumor cells, as they are both derived from ISL929, barring antigen expression, they can represent not just normal healthy cells, but also unhindered (not killed by SB CAR T cells) tumor cell growth. Then, tumor cell survival can be calculated at the endpoint with the formula: (dual antigen pink tumor cells + single antigen red tumor cells)/(n*orange cells), where n = 1 when there is only one type of tumor cell and n = 2 if both tumor cell types are present. This is effectively normalizing the number of surviving tumor cells to the theoretical endpoint number of tumor cells. This was validated by the control tumor setup: surrounding and tumor cells have similar numbers at the endpoint (SFig.8B). In the tumors without orange cells (Fig. 6C), inactivated SB CAR T cells were seeded to create control tumors with unhindered growth. Parameters modified for the challenges are given in the results section and full parameters are given in Supplementary Table 1.

4.14. Statistical analysis

Statistical testing was performed with JMP v11.0.0 with significance level of 0.05. Testing method was decided as planned comparisons before experiments were performed and Wilcoxon test was chosen due to non-parametricity of data. Samples sizes are given in the text or figures or figure captions. I show mean ± SEM.

Funding

This work was not funded by any public or private agency. This work was solely funded by the author.

CRediT authorship contribution statement

Calvin Lam: performed all the work for this study including, but not limited to, Conceptualization, Data curation, Formal analysis, Investigation, Methodology, Project administration, Resources, Software, Validation, Visualization, writing and revision of all drafts.

Declaration of competing interest

I declare no competing or financial interests.

Acknowledgements

I would like to thank UNMC for access to research articles and UNMC's printers for allowing me to print articles. I am very thankful to the three anonymous reviewer whose comments and recommendations have helped significantly improve the manuscript.

Appendix A. Supplementary data

Supplementary data to this article can be found online at https://doi.org/10.1016/j.synbio.2023.09.008.

References

[1] Santorelli M, Lam C, Morsut L. Synthetic development: building mammalian multicellular structures with artificial genetic programs. Curr Opin Biotechnol 2019;59:130–40.
[2] Lam CK, Hyde RK, Patel SA. Synthetic immunotherapy: programming immune cells with novel and sophisticated logic capabilities. Transplant Cell Ther 2022;28:560–71.
[3] Roybal KT, Lim WA. Synthetic immunology: hacking immune cells to expand their therapeutic capabilities. Annu Rev Immunol 2017;35:229–53.
[4] McNamara HM, Ramm B, Toettcher JE. Synthetic developmental biology: new tools to deconstruct and rebuild developmental systems. Semin Cell Dev Biol 2023;141:33–42.
[5] Ho C, Morsut L. Novel synthetic biology approaches for developmental systems. Stem Cell Rep 2021;16:1051–64.

[6] Martínez-Ara G, Stapornwongkul KS, Ebisuya M. Scaling up complexity in synthetic developmental biology. Science (1979) 2022;378:864–8.
[7] Kim H, Jin X, Glass DS, Riedel-Kruse IH. Engineering and modeling of multicellular morphologies and patterns. Curr Opin Genet Dev 2020;63:95–102.
[8] Toda S, Frankel NW, Lim WA. Engineering cell–cell communication networks: programming multicellular behaviors. Curr Opin Chem Biol 2019;52:31–8.
[9] Toda S, Blauch LR, Tang SKY, Morsut L, Lim WA. Programming self-organizing multicellular structures with synthetic cell-cell signaling. Science (1979) 2018;361:156–62.
[10] Lim WA, June CH. The principles of engineering immune cells to treat cancer. Cell 2017;168:724–40.
[11] Choe JH, Williams JZ, Lim WA. Engineering T cells to treat cancer: the convergence of immuno-oncology and synthetic biology. Annu Rev Cell Biol 2020;4:121–39.
[12] Caliendo F, Dukhinova M, Siciliano V. Engineered cell-based therapeutics: synthetic biology meets immunology. Front Bioeng Biotechnol 2019;7.
[13] Azimi CS, Tang Q, Roybal KT, Bluestone JA. NextGen cell-based immunotherapies in cancer and other immune disorders. Curr Opin Immunol 2019;59:79–87.
[14] Zhang C, Zhuang Q, Liu J, Liu X. Synthetic biology in chimeric antigen receptor T (CAR T) cell engineering. ACS Synth Biol 2022;11:1–15.
[15] Williams JZ, et al. Precise T cell recognition programs designed by transcriptionally linking multiple receptors. Science (1979) 2020;370:1099–104.
[16] Roybal KT, et al. Precision tumor recognition by T cells with combinatorial antigen-sensing circuits. Cell 2016;164:770–9.
[17] Zhu I, et al. Modular design of synthetic receptors for programmed gene regulation in cell therapies. Cell 2022;185:1431–1443.e16.
[18] Roybal KT, et al. Engineering T cells with customized therapeutic response programs using synthetic notch receptors. Cell 2016;167:419–432.e16.
[19] Morsut L, et al. Engineering customized cell sensing and response behaviors using synthetic notch receptors. Cell 2016;164:780–91.
[20] Toda S, et al. Engineering synthetic morphogen systems that can program multicellular patterning. Science (1979) 2020;370:327–31.
[21] Choe JH, et al. SynNotch-CAR T cells overcome challenges of specificity, heterogeneity, and persistence in treating glioblastoma. Sci Transl Med 2021;13:eabe7378.
[22] Yang Z, Yu Z, Cai Y, Du R, Cai L. Engineering of an enhanced synthetic Notch receptor by reducing ligand-independent activation. Commun Biol 2020;3:116.
[23] Saga Y. The mechanism of somite formation in mice. Curr Opin Genet Dev 2012;22:331–8.
[24] Goldbeter A, Pourquié O. Modeling the segmentation clock as a network of coupled oscillations in the Notch, Wnt and FGF signaling pathways. J Theor Biol 2008;252:574–85.
[25] Miao Y, et al. Reconstruction and deconstruction of human somitogenesis in vitro. Nature 2022. https://doi.org/10.1038/s41586-022-05655-4.
[26] Hester SD, Belmonte JM, Gens JS, Clendenon SG, Glazier JA. A multi-cell, multi-scale model of vertebrate segmentation and somite formation. PLoS Comput Biol 2011;7:e1002155.
[27] Pan G, Li J, Zhou Y, Zheng H, Pei D. A negative feedback loop of transcription factors that controls stem cell pluripotency and self-renewal. Faseb J 2006;20:1730–2.
[28] Su EW, et al. IL-2Rα mediates temporal regulation of IL-2 signaling and enhances immunotherapy. Sci Transl Med 2015;7:311ra170.
[29] Sato M, et al. Positive feedback regulation of type I IFN genes by the IFN-inducible transcription factor IRF-7. FEBS Lett 1998;441:106–10.
[30] Huang T, Irish VF. Temporal control of plant organ growth by TCP transcription factors. Curr Biol 2015;25:1765–70.
[31] Feldker N, et al. Genome-wide cooperation of EMT transcription factor ZEB1 with YAP and AP-1 in breast cancer. EMBO J 2020;39:e103209.
[32] Burrill DR, Inniss MC, Boyle PM, Silver PA. Synthetic memory circuits for tracking human cell fate. Genes Dev 2012;26:1486–97.
[33] Lam C, et al. Parameterized computational framework for the description and design of genetic circuits of morphogenesis based on contact-dependent signaling and changes in cell–cell adhesion. ACS Synth Biol 2022;11:1417–39.
[34] Swat MH, et al. Chapter 13 - multi-scale modeling of tissues using CompuCell3D. In: Asthagiri AR, Arkin AP, editors. Methods in cell biology. Academic Press; 2012. 110 325–366.
[35] Lam C, et al. Parameterized computational framework for the description and design of genetic circuits of morphogenesis based on contact-dependent signaling and changes in cell–cell adhesion. ACS Synth Biol 2022;11:1417–39.
[36] Allen GM, et al. Synthetic cytokine circuits that drive T cells into immune-excluded tumors. Science (1979) 2023;378:eaba1624.
[37] Hyrenius-Wittsten A, et al. SynNotch CAR circuits enhance solid tumor recognition and promote persistent antitumor activity in mouse models. Sci Transl Med 2021;13:eabd8836.
[38] Shaya O, et al. Cell-cell contact area affects notch signaling and notch-dependent patterning. Dev Cell 2017;40:505–511.e6.
[39] Allen GM, Lim WA. Rethinking cancer targeting strategies in the era of smart cell therapeutics. Nat Rev Cancer 2022;22:693–702.
[40] Dufva O, et al. Integrated drug profiling and CRISPR screening identify essential pathways for CAR T-cell cytotoxicity. Blood 2020;135:597–609.
[41] Singh N, et al. Impaired death receptor signaling in leukemia causes antigen-independent resistance by inducing CAR T-cell dysfunction. Cancer Discov 2020;10:552–67.
[42] Lemoine J, Ruella M, Houot R. Overcoming intrinsic resistance of cancer cells to CAR T-cell killing. Clin Cancer Res 2021;27:6298–306.
[43] Hernandez-Lopez RA, et al. T cell circuits that sense antigen density with an ultrasensitive threshold. Science (1979) 2021;371:1166–71.
[44] Wu C-Y, Roybal KT, Puchner EM, Onuffer J, Lim WA. Remote control of therapeutic T cells through a small molecule–gated chimeric receptor. Science (1979) 2015;350:aab4077.
[45] O'Donoghue GP, et al. T cells selectively filter oscillatory signals on the minutes timescale. Proc Natl Acad Sci USA 2021;118:e2019285118.
[46] Drent E, et al. Feasibility of controlling CD38-CAR T cell activity with a Tet-on inducible CAR design. PLoS One 2018;13:e0197349.
[47] Walker AJ, et al. Tumor antigen and receptor densities regulate efficacy of a chimeric antigen receptor targeting anaplastic lymphoma kinase. Mol Ther 2017;25:2189–201.
[48] Majzner RG, et al. CAR T cells targeting B7-H3, a pan-cancer antigen, demonstrate potent preclinical activity against pediatric solid tumors and brain tumors. Clin Cancer Res 2019;25:2560–74.
[49] Lemoine J, Ruella M, Houot R. Born to survive: how cancer cells resist CAR T cell therapy. J Hematol Oncol 2021;14:199.
[50] Grupp SA, et al. Chimeric antigen receptor–modified T cells for acute lymphoid leukemia. N Engl J Med 2013;368:1509–18.
[51] Chen GM, et al. Characterization of leukemic resistance to CD19-targeted CAR T-cell therapy through deep genomic sequencing. Cancer Immunol Res 2023;11:13–9.
[52] Srivastava S, Riddell SR. Engineering CAR-T cells: design concepts. Trends Immunol 2015;36:494–502.
[53] Salinas RD, Durgin JS, O'Rourke DM. Potential of glioblastoma-targeted chimeric antigen receptor (CAR) T-cell therapy. CNS Drugs 2020;34:127–45.
[54] Majzner RG, Mackall CL. Tumor antigen escape from CAR T-cell therapy. Cancer Discov 2018;8:1219–26.
[55] O'Rourke DM, et al. A single dose of peripherally infused EGFRvIII-directed CAR T cells mediates antigen loss and induces adaptive resistance in patients with recurrent glioblastoma. Sci Transl Med 2017;9:eaaa0984.
[56] Song D-G, et al. Effective adoptive immunotherapy of triple-negative breast cancer by folate receptor-alpha redirected CAR T cells is influenced by surface antigen expression level. J Hematol Oncol 2016;9:56.
[57] Prybutok AN, Yu JS, Leonard JN, Bagheri N. Mapping CAR T-cell design space using agent-based models. Front Mol Biosci 2022;9.
[58] Zhang Z, Liu L, Ma C, Chen W. A computational model of cytokine release syndrome during CAR T-cell therapy. Adv Ther 2022;5:2200130.
[59] Liu L, et al. Computational model of CAR T-cell immunotherapy dissects and predicts leukemia patient responses at remission, resistance, and relapse. J Immunother Cancer 2022;10:e005360.
[60] Fischel H, Giorgadze T, Tessier A, Norton K-A. Computational modeling of chimeric antigen receptor (CAR) T-cell therapy of a binary model of antigen receptors in breast cancer. In: 2021 IEEE international conference on bioinformatics and biomedicine (BIBM); 2021. p. 3267–74. https://doi.org/10.1109/BIBM52615.2021.9669393.
[61] Rohrs JA, Wang P, Finley SD. Understanding the dynamics of T-cell activation in health and disease through the lens of computational modeling. JCO Clin Cancer Inform 2019:1–8. https://doi.org/10.1200/CCI.18.00057.
[62] Lienert F, Lohmueller JJ, Garg A, Silver PA. Synthetic biology in mammalian cells: next generation research tools and therapeutics. Nat Rev Mol Cell Biol 2014;15:95–107.
[63] Ajo-Franklin CM, et al. Rational design of memory in eukaryotic cells. Genes Dev 2007;21:2271–6.
[64] Becskei A, Séraphin B, Serrano L. Positive feedback in eukaryotic gene networks: cell differentiation by graded to binary response conversion. EMBO J 2001;20:2528–35.
[65] To T-L, Maheshri N. Noise can induce bimodality in positive transcriptional feedback loops without bistability. Science (1979) 2010;327:1142–5.
[66] Haynes KA, Silver PA. Synthetic reversal of epigenetic silencing. J Biol Chem 2011;286:27176–82.
[67] Cabrera A, et al. The sound of silence: transgene silencing in mammalian cell engineering. Cell Syst 2022;13:950–73.
[68] Hartfield RM, Schwarz KA, Muldoon JJ, Bagheri N, Leonard JN. Multiplexing engineered receptors for multiparametric evaluation of environmental ligands. ACS Synth Biol 2017;6:2042–55.
[69] Zhou J, Ge Q, Wang D, Guo Q, Tao Y. Engineering a modular double-transmembrane synthetic receptor system for customizing cellular programs. Cell Rep 2023;42.
[70] Chen Z, Elowitz MB. Programmable protein circuit design. Cell 2021;184:2284–301.
[71] Javdan SB, Deans TL. Design and development of engineered receptors for cell and tissue engineering. Curr Opin Struct Biol 2021;28:100363.
[72] Barnea G, et al. The genetic design of signaling cascades to record receptor activation. Proc Natl Acad Sci USA 2008;105:64–9.
[73] Daringer NM, Dudek RM, Schwarz KA, Leonard JN. Modular extracellular sensor architecture for engineering mammalian cell-based devices. ACS Synth Biol 2014;3:892–902.
[74] Schwarz KA, Daringer NM, Dolberg TB, Leonard JN. Rewiring human cellular input–output using modular extracellular sensors. Nat Chem Biol 2017;13:202–9.
[75] Pistikou A-MM, et al. Engineering a scalable and orthogonal platform for synthetic communication in mammalian cells. bioRxiv 2023:524631. https://doi.org/10.1101/2023.01.18.524631. 2023.01.18.
[76] Kipniss NH, et al. Engineering cell sensing and responses using a GPCR-coupled CRISPR-Cas system. Nat Commun 2017;8:2212.

[77] Edelstein HI, et al. Elucidation and refinement of synthetic receptor mechanisms. Synth Biol 2020;5:ysaa017.
[78] Albinger N, Hartmann J, Ullrich E. Current status and perspective of CAR-T and CAR-NK cell therapy trials in Germany. Gene Ther 2021;28:513–27.
[79] Klichinsky M, et al. Human chimeric antigen receptor macrophages for cancer immunotherapy. Nat Biotechnol 2020;38:947–53.
[80] Gumbiner BM. Cell adhesion: the molecular basis of tissue architecture and morphogenesis. Cell 1996;84:345–57.
[81] Takeichi M. Self-organization of animal tissues: cadherin-mediated processes. Dev Cell 2011;21:24–6.
[82] Alberts B, et al. Molecular biology of the cell. Garland Science; 2002. 10.1002.
[83] Persson J, Mölder AL, Pettersson S-G, Alm K. Cell motility studies using digital holographic microscopy. 2010.
[84] Reeve R, Turner JR. Pharmacodynamic models: parameterizing the Hill equation, michaelis-menten, the logistic curve, and relationships among these models. J Biopharm Stat 2013;23:648–61.
[85] Zhu R, del Rio-Salgado JM, Garcia-Ojalvo J, Elowitz MB. Synthetic multistability in mammalian cells. Science (1979) 2023;375:eabg9765.
[86] Barlow R, Blake JF. Hill coefficients and the logistic equation. Trends Pharmacol Sci 1989;10:440–1.
[87] Prinz H. Hill coefficients, dose–response curves and allosteric mechanisms. J Chem Biol 2010;3:37–44.
[88] Hutson MS, Leung MCK, Baker NC, Spencer RM, Knudsen TB. Computational model of secondary palate fusion and disruption. Chem Res Toxicol 2017;30:965–79.
[89] Anderson ARA. A hybrid mathematical model of solid tumour invasion: the importance of cell adhesion. Math Med Biol 2005;22:163–86.
[90] Dogu Y, Díaz J. Mathematical model of a network of interaction between p53 and Bcl-2 during genotoxic-induced apoptosis. Biophys Chem 2009;143:44–54.
[91] McKenna S, García-Gutiérrez L, Matallanas D, Fey D. BAX and SMAC regulate bistable properties of the apoptotic caspase system. Sci Rep 2021;11:3272.
[92] Ho KL, Harrington HA. Bistability in apoptosis by receptor clustering. PLoS Comput Biol 2010;6:e1000956.
[93] MacLachlan TK, El-Deiry WS. Apoptotic threshold is lowered by p53 transactivation of caspase-6. Proc Natl Acad Sci USA 2002;99:9492–7.
[94] Legewie S, Blüthgen N, Herzel H. Mathematical modeling identifies inhibitors of apoptosis as mediators of positive feedback and bistability. PLoS Comput Biol 2006;2:e120.
[95] Kracikova M, Akiri G, George A, Sachidanandam R, Aaronson SA. A threshold mechanism mediates p53 cell fate decision between growth arrest and apoptosis. Cell Death Differ 2013;20:576–88.